

This is a repository copy of *Biochemical characterization and low-resolution SAXS shape of a novel GH11 exo-1,4- $\beta$ -xylanase identified in a microbial consortium*.

White Rose Research Online URL for this paper:

<https://eprints.whiterose.ac.uk/148947/>

Version: Accepted Version

---

**Article:**

Evangelista, Danilo Elton, de Oliveira Arnoldi Pellegrini, Vanessa, Espirito Santo, Melissa et al. (3 more authors) (2019) Biochemical characterization and low-resolution SAXS shape of a novel GH11 exo-1,4- $\beta$ -xylanase identified in a microbial consortium. APPLIED MICROBIOLOGY AND BIOTECHNOLOGY. pp. 8035-8049. ISSN 0175-7598

<https://doi.org/10.1007/s00253-019-10033-8>

---

**Reuse**

Items deposited in White Rose Research Online are protected by copyright, with all rights reserved unless indicated otherwise. They may be downloaded and/or printed for private study, or other acts as permitted by national copyright laws. The publisher or other rights holders may allow further reproduction and re-use of the full text version. This is indicated by the licence information on the White Rose Research Online record for the item.

**Takedown**

If you consider content in White Rose Research Online to be in breach of UK law, please notify us by emailing [eprints@whiterose.ac.uk](mailto:eprints@whiterose.ac.uk) including the URL of the record and the reason for the withdrawal request.

1 **Biochemical characterization and low-resolution SAXS shape of a novel GH11 exo-1,4- $\beta$ -xy lanase**  
2 **identified in a microbial consortium**

3

4 **Danilo Elton Evangelista<sup>1a</sup>, Vanessa de Oliveira Arnoldi Pellegrini<sup>1a</sup>, Melissa Espirito Santo<sup>1</sup>, Simon**  
5 **McQueen-Mason<sup>2</sup>, Neil C. Bruce<sup>2</sup> and Igor Polikarpov<sup>1\*</sup>.**

6

7 <sup>1</sup>Instituto de Física de São Carlos, Universidade de São Paulo, Avenida Trabalhador São-carlense 400,  
8 13566-590 São Carlos – SP, Brazil.

9 <sup>2</sup>Department of Biology, University of York, Wentworth Way, York, UK, YO10 5DD

10 <sup>a</sup>These authors contributed equally to this work

11

12 \*Correspondent author: [ipolikarpov@ifsc.usp.br](mailto:ipolikarpov@ifsc.usp.br)

13

14 **ACKNOWLEDGEMENTS**

15 The authors acknowledge Dr. Marco A. S. Kadowaki for his help with HPAEC analysis and Dr.  
16 Evandro Ares de Araújo for assistance with SAXS data collection and processing.

17

18

19

20

21

22 **Abstract**

23 Biotechnologies that aim to produce renewable fuels, chemicals, and bioproducts from residual  
24 ligno(hemi)cellulosic biomass mostly rely on enzymatic depolymerization of plant cell walls (PCW). This  
25 process requires an arsenal of diverse enzymes, including xylanases, which synergistically act on the  
26 hemicellulose, reducing the long and complex xylan chains to oligomers and simple sugars. Thus, xylanases  
27 play a crucial role in PCW depolymerization. Until recently, the largest xylanase family, glycoside  
28 hydrolase family 11 (GH11) has been exclusively represented by endo-catalytic  $\beta$ -1,4- and  $\beta$ -1,3-xylanases.  
29 Analysis of a metatranscriptome library from a microbial lignocellulose community resulted in the  
30 identification of an unusual exo-acting GH11  $\beta$ -1,4-xylanase (MetXyn11). Detailed characterization has  
31 been performed on recombinant MetXyn11 including determination of its low-resolution small angle X-  
32 ray scattering (SAXS) molecular envelope in solution. Our results reveal that MetXyn11 is a monomeric  
33 globular enzyme that liberates xylobiose from heteroxylans as the only product. MetXyn11 has an optimal  
34 activity in a pH range from 6 to 9 and an optimal temperature of 50 °C. The enzyme maintained above 65%  
35 of its original activity in the pH range 5 to 6 after being incubated for 72 h at 50 °C. Addition of the enzyme  
36 to a commercial enzymatic cocktail (CelicCtec3) promoted a significant increase of enzymatic hydrolysis  
37 yields of hydrothermally pretreated sugarcane bagasse (16% after 24 h of hydrolysis).

38 **Keywords:** GH11 exo- $\beta$ -1,4-xylanase; Metatranscriptome; Biochemical characterization; Synergism;  
39 Small Angle X-ray Scattering.

40

41

## 42 INTRODUCTION

43 Use of residual plant biomass as a feedstock for the production of biofuel, chemicals, and  
44 renewable materials, represents a feasible, sustainable and environmentally friendly alternative to fossil  
45 fuel-derived products (Isikgor and Becer 2015; Sims et al. 2010; Silva et al. 2018). Conversion of plant  
46 residues into these products relies on the controlled deconstruction and depolymerization of plant cell walls  
47 (PCW) (Keegstra 2010). Because of the intricate ultrastructure and diversified linkage complexity of PCW,  
48 efficient enzymatic processing of biomass-based feedstocks remains a challenge (Isikgor and Becer 2015;  
49 Johnson 2016; Silva et al. 2018). The enzymatic depolymerization of PCW is currently one of the most  
50 expensive technological steps in its valorization (Johnson 2016). Existing enzyme cocktails comprise  
51 mixtures of different plant cell wall degrading enzymes (PCWDE), each one with a distinct mechanism of  
52 action that synergistically reduce the PCW into simple sugars (Silva et al. 2018). Therefore, in order to  
53 decrease associated costs and increase efficiency, there is a constant demand for new enzymes with  
54 biochemical and biophysical properties that match industrial requirements, such as thermal and pH stability,  
55 activity at a broad pH range, and different substrate specificities or new mechanisms of activity, to list a  
56 few. Our current knowledge of enzymatic deconstruction of PCWs is incomplete and the discovery and  
57 characterization of new enzymes with novel catalytic mechanisms will contribute to a better understanding  
58 of PCW depolymerization.

59 Although PCWDE have been characterized from plants (Johansson et al. 2002; Suzuki et al. 2002)  
60 and animals (Evangelista et al. 2015; Watanabe and Tokuda 2001; Pauchet et al. 2010), microorganisms  
61 represent the main source for enzyme discovery. In this context, metatranscriptomic studies on complex  
62 unculturable microbial communities have greatly enhanced the pace of identification of enzymes from  
63 underexplored and uncultivable microorganisms (Castillo et al. 2013; Rittmann et al. 2006; Curtis et al.  
64 2003; Duan and Feng 2010). For these reasons, we have conducted metatranscriptomic studies of a  
65 microbial consortium, which was grown in a nutrient-limited medium enriched with sugarcane bagasse,  
66 to selectively favor microorganisms capable of degrading PCW (Mello et al. 2016; Evangelista et al.  
67 2018). In the course of these studies, a GH11 exo-acting  $\beta$ -1,4-xylanase, termed here MetXyn11, was  
68 identified (GenBank accession number: ATY75129.1).

69 Xylanases cooperatively act on xylan (the major component of hemicellulose), which is composed  
70 of a linear backbone chain of xylopyranose residues linked by  $\beta$ -1,4 glycosidic bonds and decorated with

71  $\beta$ -D-galactopyranosyl,  $\alpha$ -L-arabinofuranosyl, and  $\alpha$ -D-glucuronic acid or its 4-*O*-methyl ether derivative  
72 residues (Pollet et al. 2010; Paës et al. 2012; Kalim et al. 2015; Biely et al. 2016). Due to their essential  
73 participation in biomass depolymerization, xylanases have been widely applied in several industrial sectors,  
74 such as second-generation bioethanol production; prebiotic production; pulp treatment; xylitol production;  
75 industrial waste treatment; and degumming of fibers for paper and textiles, to name a few (Kalim et al.  
76 2015; Paës et al. 2012). Xylanases from GH10 and GH11 families are the most studied and widely used in  
77 biotechnological applications. In contrast to other GH families that comprise xylanases, GH11 is known as  
78 “true  $\beta$ -1,4-xylanase” family, because it is almost entirely composed of  $\beta$ -1,4-xylanases (Kalim et al. 2015;  
79 Paës et al. 2012). Moreover, until very recently, all GH11 members had been characterized as endo-catalytic  
80 enzymes that are highly specific for cleaving the internal linkages of the heteroxylans. However, our group  
81 recently identified the first GH11 with exo- $\beta$ -1,4-xylanase activity (Mello et al., 2016).

82 Considering the essential role of xylanases in PCW depolymerization and biotechnological  
83 applications of these enzymes, here we report the identification and detailed characterization of a second  
84 GH11 family member (MetXyn11) that displays exo- $\beta$ -1,4-xylanase activity, and demonstrate its ability to  
85 significantly increase sugar release when added to a commercial cellulase cocktail.

86

## 87 **MATERIALS AND METHODS**

### 88 **Cloning, heterologous expression, and purification**

89 MetXyn11 was identified from a previously reported metatranscriptomic library (Mello et al. 2016;  
90 Evangelista et al. 2018). Its amino acid sequence was analyzed using BLASTP (Altschul et al. 1990),  
91 ExPASy (Wilkins et al. 1999), XtalPred (Slabinski et al. 2007) and SignalP 4.0 (Petersen et al. 2011)  
92 software. The MetXyn11 open reading frame (ORF), devoid of the signal peptide coding sequence, was  
93 cloned into the expression vector pETM11/LIC, using the ligation independent cloning (LIC) method  
94 (Camilo and Polikarpov 2014). First, the DNA sequence target was amplified by PCR, in which the  
95 genomic DNA extracted from the microbial consortia was used as a template. The following primers were  
96 designed to amplify MetXyn11 sequence (LIC tails are shown in italic): MetXyn11\_Forward 5’-  
97 *CAGGGCGCCATGGAACCCAAAATGCCACCTG*-3’ and MetXyn11\_Reverse 5’-  
98 *GACCCGACGCGGTAAACGGGGTGTTCATCCC*-3’. The resulting plasmid was designed to express

99 MetXyn11 fused with a 6xHis-tag at the N-terminal region, including a cleavage site for *Tobacco etch* virus  
100 protease (TEV) between the two sequences (Camilo and Polikarpov 2014). This allows the proteolytic  
101 6xHis-tag removal after the protein purification by Ni<sup>+2</sup> affinity chromatography. The resulting plasmid  
102 was propagated in *Escherichia coli* (DH5 $\alpha$ ) cells (Thermofischer, Waltham USA), and the purified plasmid  
103 was used in the heat-shock transformation of *E. coli* Rosetta (DE3) cells (Novagen, Watertown USA) to  
104 create the MetXyn11 expression strain.

105 MetXyn11 expression was carried out in LB medium at 37 °C for 5 h (O.D.<sub>600</sub> = 0.6), followed by  
106 an induction step at 18 °C for 24 h, containing 1 mM IPTG. The cells were pelleted at 2.500  $\times$  g for 45 min  
107 at 4 °C, suspended in lyses buffer (50 mM Tris pH 8.0, 150 mM NaCl, 4 mM PMSF, 2 mM DTT, 10%  
108 (v/v) glycerol and 50  $\mu$ g.mL<sup>-1</sup> of lysozyme), incubated at 18 °C for 20 min and sonicated on an ice bath  
109 using a 550 Sonic Dismembrator Sonifier (Fisher Scientific, Hampton USA). Next, the cells were pelleted  
110 (6,000  $\times$  g, 45 min at 4 °C) and the supernatant was used for MetXyn11 protein purification.

111 Three chromatographic steps were used for MetXyn11 purification: two steps of Ni<sup>+2</sup> affinity  
112 chromatography, one before and one after TEV proteolysis; and a third step of size exclusion  
113 chromatography. In the first step, MetXyn11 (~30 kDa) attached to 6xHis-tag was eluted using 50 mM Tris  
114 pH 8.0, 150 mM NaCl and 125 mM imidazole. The sample was dialyzed to remove traces of imidazole and  
115 then, incubated with 3 mg.mL<sup>-1</sup> of TEV protease at 4 °C for 48 h. In the second purification step, MetXyn11  
116 (~29 kDa) free of 6xHis-tag was eluted in 50 mM Tris pH 8.0 and 150 mM NaCl. The third purification  
117 step was conducted on a Superdex<sup>TM</sup> 75 prep grade 16/60 (GE-Healthcare, Chicago USA) gel filtration  
118 column equilibrated with 50 mM Tris pH 8.0 and 150 mM NaCl. The protein was concentrated to 1 mg.mL<sup>-1</sup>  
119 <sup>1</sup>, using the 10 kDa Vivaspin Concentrator (GE-Healthcare, Chicago USA) at 1,500  $\times$  g and stocked at 4  
120 °C. The protein integrity and sample purity were confirmed by the 15% SDS-PAGE (sodium dodecyl  
121 sulfate–polyacrylamide gel electrophoresis) analysis.

## 122 **Thermofluor assays**

123 To determine the best condition for the enzyme storage and handling, the enzyme's thermal stability  
124 was evaluated using in several different buffered solutions using a thermal shift fluorescence (Thermofluor)  
125 assay (Table S1, Supplementary Materials). Moreover, we also assessed the MetXyn11 tertiary structure  
126 stability in different pH conditions, using the 50 mM sodium acetate/ borate/ phosphate (ABF) buffer in a  
127 pH range from pH 2 to 10. The experiments consisted of 20  $\mu$ L reaction containing 13  $\mu$ M of the enzyme

128 in 50 mM buffer with 5  $\mu$ L of SYPRO Orange dye 10X (Invitrogen, Carlsbad USA). Reactions were  
129 performed in triplicate in a 96-well thin-wall PCR plate (Bio-Rad, Hercules USA). The plate was sealed  
130 with Optical-Quality Sealing Tape (Bio-Rad, Hercules USA), then incubated in an iCycler iQ Real-Time  
131 PCR Detection System (Bio-Rad, Hercules USA). The temperature ranged from 25 to 90  $^{\circ}$ C, increasing 1  
132  $^{\circ}$ C per minute, added of a holding step of 30 seconds at each point. The extrinsic fluorescence from the  
133 probe was measured at 490/530 nm of excitation/emission wavelengths. The melting temperature ( $T_m$ ) was  
134 calculated by Boltzmann sigmoidal function, using the GraphPad Prism 6.0 software (GraphPad Software  
135 Inc., La Jolla USA).

### 136 **Enzymatic assays**

137 The MetXyn11 enzymatic activity was quantified by the DNS method that measures the reducing end-  
138 groups of saccharides (Miller 1959). All experiments were conducted in triplicate. Enzyme specificity was  
139 assessed using 15 different substrates: Avicel, carboxymethylcellulose, Sigmacell20 and  
140 hydroxyethylcellulose (all from Sigma, St. Louis USA); glucuronoxylan from beechwood; arabinoxylan  
141 from rye flour, arabinan, debranched arabinan,  $\beta$ -glucan, xyloglucan, dextrin, galactomannan, larch  
142 arabinogalactan, lichenan and mannan (all from Megazyme, Bray, Republic of Ireland). Since MetXyn11  
143 showed significant activity only against glucuronoxylan, this substrate was used for the subsequent  
144 biochemical experiments. The reaction consisted of 35 nM of enzyme mixed with 1% (w/v) glucuronoxylan  
145 and 50 mM buffer ions in 50  $\mu$ L final volume, which was incubated for 10 min. The reaction was stopped  
146 by the addition of 100  $\mu$ l of DNS reagent and heating at 95  $^{\circ}$ C for 10 min, followed by cooling on ice for 1  
147 min for color stabilization. Product absorbance was measured at 540 nm using the MultiSkan Spectrum  
148 equipment (Thermo Scientific, Waltham USA), and a standard concentration curve of D-(+)-xylose (Sigma,  
149 St. Louis USA) was used to express results in reducing sugars equivalents. All the obtained data were  
150 analyzed using the GraphPad Prism 6.0 software (GraphPad Software Inc., La Jolla USA).

151 The optimum pH was evaluated in pH range from 2 to 10 in ABF buffer at 50  $^{\circ}$ C. The optimal  
152 temperature was assessed in a potassium phosphate buffered solution at 50 mM concentration and pH 7.0  
153 in a temperature range from 30 to 70  $^{\circ}$ C. In both sets of experiments the reactions were performed as  
154 described above. Moreover, enzyme stability assays were performed, quantifying MetXyn11 residual  
155 activity after enzyme pre-incubation under long periods in different temperatures or pHs. During the  
156 thermal stability assays MetXyn11 was kept at 50  $^{\circ}$ C in potassium phosphate buffer pH 6.0 for 120 h. For

157 the pH stability assay, MetXyn11 was maintained in ABF buffer at pH range from 2 to 10 at 50 °C for 72  
158 h. The residual activity was measured under the optimal temperature and buffer conditions. Furthermore,  
159 under the optimal conditions, the enzyme activity was also evaluated upon addition of 15 different chemical  
160 compounds (Table S2, Supplementary Materials). To evaluate enzyme kinetics, the reactions were  
161 performed under the optimal conditions enzymatic activity, varying glucuronoxylan concentration from 0.1  
162 to 18 mg.mL<sup>-1</sup>

#### 163 **Enzymatic cleavage pattern determined by high-performance anion exchange chromatography** 164 **(HPAEC)**

165 The soluble products released by the MetXyn11 catalytic action on heteroxylans (glucuronoxylan and  
166 arabinoxylan) and on xylohexaose were analyzed using HPAEC. In experiments with heteroxylans,  
167 reactions containing 1% of substrate and 35 nM of MetXyn11 were conducted under optimal conditions  
168 for 24 h. For comparison, we also performed experiments using a typical endo-1,4-β-xylanase  
169 (rGH11Xyn11B; Ghio et al. 2017) instead of MetXyn1, to compare their heteroxylan cleavage pattern. In  
170 the experiments with xylohexaose, the reactions were conducted with 55 μM of substrate and analyzed in  
171 1, 5, 10 and 15 min time points. A pool containing 5 μL of each reaction conducted in triplicate was diluted  
172 10-fold, then centrifuged at 13,000 *x g* for 5 min and the supernatant was analyzed by a DIONEX ICS3000  
173 instrument (DIONEX, Sunnyvale USA) connected to a CarboPac PA1 4 X 250 mm column (DIONEX,  
174 Sunnyvale USA). The column was equilibrated with 100 mM NaOH at 1 mL.min<sup>-1</sup> for 5 min; the sugars  
175 were separated using a gradient from 100 mM NaOH/0 mM NaAc to 100 mM NaOH/150 mM NaAc over  
176 20 minutes.

#### 177 **Supplementation of commercial enzymatic cocktail for pretreated plant biomass saccharification**

178 Hydrothermally pretreated sugarcane bagasse was used in saccharification assays with Celic CTec3 ±  
179 MetXyn11. The biomass was provided by the Raízen Group (Costa Pinto/Piracicaba, São Paulo, Brazil).  
180 The raw material was rinsed with hot water (50 °C ± 5 °C) and milled using a knife mill. Next, it was dried  
181 in the oven at 60 °C for 24 h and hydrothermally pretreated.

182 Hydrothermal pretreatment was performed using hot water for 30 minutes at 160 °C in a pretreatment  
183 reactor AU/E-20 model (Regmed, Osasco Brazil). The pressure was kept at 7 bar and a 1:10 solid to liquid  
184 ratio (grams of bagasse/mL of water) was used (Santo et al. 2018). The pretreated sugarcane bagasse used  
185 in the study contained 76.8% ± 1.5% of glucan, 6.1% ± 0.1% of xylan, 17.8% ± 0.5% of lignin and 1.4% ±

186 0.02% of ash content. The saccharification of pretreated sugarcane bagasse was carried out at a substrate  
187 concentration of 10% (w/v). Cellic CTec3 (Novozymes, Kalundborg DKK) protein loading was 5 mg/g of  
188 substrate in the control reactions. To evaluate effect of MetXyn11 supplementation 0.125 mg of the enzyme  
189 per g of substrate was added to Cellic CTec3 reaction. The reactions were conducted in a citrate buffer (50  
190 mM, pH 5.0), at 50 °C up to 72 h. The soluble hydrolysate products were analyzed by high performance  
191 liquid chromatography (HPLC) (Shimadzu, Kyoto Japan), equipped with refractive index detector and UV-  
192 VIS spectrophotometer. Aminex HPX-87 H (Bio-Rad, Hercules USA) column was used and 5 mM H<sub>2</sub>SO<sub>4</sub>  
193 solution at 65 °C was utilized as a mobile phase (flow rate 0.6 mL.min<sup>-1</sup>). Glucose and xylose were used as  
194 standards.

### 195 **Homology modelling of MetXyn11**

196 A multiple alignment was performed, using T-Coffee Server (Notredame et al. 2000), for comparative  
197 analyses between MetXyn11 amino acid sequence and some of the traditional GH11 endo-β-1,4-xylanases,  
198 and also Compost21\_GH11 enzyme, that represents the unique previously reported GH11 exo-β-1,4-  
199 xylanase (Mello et al. 2016). Moreover, a three-dimensional (3D) homology model of MetXyn11 was  
200 generated using the MetXyn11 amino acid sequence and using the Compost21\_GH11 crystal structure  
201 (PDB id: 5VQJ) as inputs in the I-Tasser software (Yang et al. 2015). Following this, the 3D homology  
202 model was superimposed with the crystal structures of the GH11 members used in our amino acid sequences  
203 alignment, using Pymol program (DeLano 2002)

### 204 **SAXS studies**

205 Small angle X-ray scattering (SAXS) experiments were carried out at the D02A-SAXS1 beamline of  
206 the Brazilian Synchrotron Light Laboratory (LNLS, Campinas, Brazil). To remove protein aggregates,  
207 samples (at the concentrations of 1, 7.5 and 15 mg.mL<sup>-1</sup> in 50 mM potassium phosphate pH 7.0 and 150  
208 mM NaCl) were centrifuged at 17,000 *x* g for 5 min at 4 °C prior to measurements, and the supernatant was  
209 collected. Next, the supernatant was loaded in a 1 mm path-length capillary cell and exposed to X-rays  
210 during 10 frames of 30 s, with intervals of 1 s between each frame. The data sets were collected using a  
211 monochromatic X-ray beam ( $\lambda= 1.55 \text{ \AA}$ ) with a Pilatus 300 area detector (Dectris, Baden Switzerland). To  
212 cover a scattering vector ( $q=4\pi/\lambda\sin(\theta)$ , being  $2\theta$  the scattering angle) range from 0.012 to 0.400  $\text{\AA}^{-1}$ , the  
213 distance between sample and detector was adjusted to ~1,000 mm. The scattering from buffer alone was  
214 subtracted from the sample's scattering. Comparative analysis between each frame was used to verify

215 radiation damage. Guinier analysis (Guinier and Fournet 1955; Konarev and Svergun 2015; Perry and  
216 Tainer 2013) was applied to verify monodispersivity and to calculate the radius of gyration ( $R_g$ ), which was  
217 also estimated by an indirect Fourier transform method, using the GNOM program (Svergun 1992). The  
218 distance distribution function  $P(r)$  was analyzed by GNOM and the maximum particle dimension ( $D_{max}$ )  
219 was determined. Ten ab initio envelope models were generated by DAMMIN (Franke et al. 2009), then  
220 aligned and averaged by DAMAVER (Volkov and Svergun 2003), to build the final MetXyn11 molecular  
221 envelope. The 3D-homology model of MetXyn11 structure was inputted into Crysol online software  
222 (Svergun et al. 1995) to generate a theoretical SAXS profile, which was compared to the experimental  
223 SAXS profile. Moreover, the 3D-homology model of MetXyn11 structure and the final model of MetXyn11  
224 molecular envelope were superimposed by SUPCOMB program (Kozin and Svergun 2001).

225

## 226 **RESULTS**

### 227 **Bioinformatic analysis**

228 Bioinformatic analysis revealed that MetXyn11 has 268 amino acid residues (including a putative 21-  
229 residue signal peptide) and a molecular mass of ~28 kDa. The enzyme has a calculated isoelectric point of  
230 6.22. MetXyn11 has the highest amino acid sequence similarity (id > 80%) with Compost21\_GH11 (PDB  
231 id: 5VQJ) and another GH11 exo- $\beta$ -1,4-xylanase (GenBank: ATY75130.1), identified in the same  
232 metatranscriptomic library. The organism(s) that carries (carry) these exo- $\beta$ -1,4-xylanase genes is(are) still  
233 unknown, however, MetXyn11 also shows high similarity to other known GH11 endo- $\beta$ -1,4-xylanase from  
234 bacterial sources, particularly with the enzymes from the *Cellvibrio* genus including *Cellvibrio* sp.  
235 PSBB006, *Cellvibrio mixtus*, *Cellvibrio* sp. PSBB023 and *Cellvibrio* sp. pealriver (all with id = 78%).

236 Comparative analyses between the amino acid sequences and 3D structures of MetXyn11,  
237 Compost21\_GH11 and some typical GH11 endo- $\beta$ -1,4-xylanases revealed some notable differences  
238 between these enzymes (Fig. 1). The first noticeable difference between these enzymes is the extended  
239 amino acid sequence at the N-terminus of MetXyn11, which was predicted as being an extra  $\alpha$ -helix. The  
240 second difference between these enzymes, is the two extra loops shared by MetXyn11 and  
241 Compost21\_GH11, which are absent in typical GH11 endo- $\beta$ -1,4-xylanases.

### 242 **Cloning, heterologous expression and purification**

243 MetXyn11 ORF was cloned into the pETM11/LIC expression vector, and used to transform *E. coli*  
244 Rosetta cells. The enzyme was successfully overexpressed as a soluble protein fused to the 6xHis-tag (Fig.  
245 2). The enzyme was purified in three purification steps and eluted as a single peak after size exclusion  
246 chromatography, confirming sample purity. The MetXyn11 molecular mass estimated by SDS-PAGE (~28  
247 kDa) is in agreement with the theoretical molecular mass predicted from its amino acid sequence (Fig. 2).

#### 248 **Substrate specificity and hydrolytic products**

249 MetXyn11 specific activity was tested against 15 different plant polysaccharides. Among all the  
250 tested potential substrates, the enzyme showed detectable enzymatic activity only against glucuronoxylan  
251 and arabinoxylan. MetXyn11 has a much higher activity for glucuronoxylan than to arabinoxylan. Indeed,  
252 as evaluated by the DNS method, MetXyn11 exhibited a 50 times lower specific activity for arabinoxylan  
253 when compared to glucuronoxylan. To evaluate the products released by MetXyn11 on these substrates,  
254 we analyzed them using HPAEC-PAD (Fig. 3). For both substrates, the enzyme released xylobiose as the  
255 unique product, indicating an exo catalytic pattern. For comparison both substrates were also hydrolysed  
256 by *Paenibacillus* sp. A59 GH11 endoxylanase (rGH11XynB; Ghio et al., 2018) kindly donated by Prof.  
257 Eleonora Campos (INTA, Argentina), revealing strikingly different hydrolytic patterns. Liberation of  
258 xylobiose by MetXyn11 was also confirmed by the experiments using xylohexaose as a substrate (Fig. 4).  
259 In these experiments, the profile of xylo-oligosaccharides evaluated over the 15 min of reaction revealed  
260 the conversion of xylohexaose into xylotetraose plus xylobiose, then, the conversion of xylotetraose to  
261 xylobiose. Since the xylohexaose used here had a small amount of xylopentaose contamination (Fig. S1,  
262 Supplementary Materials), it was also possible to observe the conversion of the xylopentaose in xylotriase  
263 plus xylobiose.

#### 264 **Optimal conditions for MetXyn11 stability**

265 Optimal conditions for MetXyn11 stability were determined by assessing its tertiary structural  
266 integrity in several different buffer solutions at different temperatures by Thermofluor analysis (Ericsson  
267 et al. 2006) (Table S1, Supplementary Materials). The results showed a good fit with the Boltzmann  
268 sigmoidal equation, which is usually applied for non-linear fitting of thermal denaturation data, revealing  
269 that MetXyn11 tertiary structure has a  $T_m$  value of 55 °C in its best buffer conditions (Fig. 5). MetXyn11 is  
270 most stable between pHs 5.5 and 7.0, in sodium phosphate pH 5.5, MES pH 5.8-6.5, Bis-Tris pH 6.0-7.0  
271 and HEPES pH 7.0 ( $T_m = 55$  °C) buffers, followed by several other buffers with pHs between 4.7 and 8.5

272 ( $T_m = 51-54$  °C). The enzyme was least stable at the extreme pHs: HCl pH 2.0 ( $T_m = 26$  °C), citric acid pH  
273 3.0 ( $T_m = 46$  °C) and sodium carbonate pH 9.5-10.0 ( $T_m = 46$  °C).

#### 274 **Effects of metal ions and chemicals on enzyme activity**

275 MetXyn11 activity was evaluated in the presence of different metal ions and chemicals (Table S2,  
276 Supplementary Materials). The major detrimental effects were observed for SDS (sodium dodecyl sulfate)  
277 and  $Fe^{+3}$  that completely inactivated the enzyme, followed by  $Mn^{+2}$ ,  $Fe^{+2}$ ,  $Cu^{+2}$ ,  $Co^{+2}$  and  $Ca^{+2}$  which  
278 imparted a loss of approximately 78%, 46%, 46%, 21% and 20% of its catalytic activity, respectively. In  
279 contrast,  $Li^{+2}$ ,  $Ni^{+2}$ ,  $K^+$  and  $Mg^{+2}$  enhanced MetXyn11 activity by approximately 6%, 10%, 12% and 23%,  
280 respectively. Neutral surfactants, Tween-20 and Triton-100X respectively provoked a loss of 16.5 % and a  
281 gain of 8% on MetXyn11 activity, respectively. The reducing agents DTT and  $\beta$ -mercaptoethanol caused  
282 decrease of the enzyme activity equal to 15% and 5%, respectively.

#### 283 **MetXyl11 optimal activity and the enzyme kinetics**

284 MetXyn11 activity was highest around 50 °C; however, the enzyme maintained over 80% of its  
285 optimal activity at both 40 °C and 60 °C (Fig. 6A). We also determined the MetXyn11 activity profile  
286 following variations of pH. The enzyme showed the best performance at pH 6-7, retaining above 60% of  
287 the maximum activity at pH 5, approximately 90% at pH 8-9 and 80% at pH 10. No significant activity was  
288 detected at pHs below 5 (Fig. 6B). According to the BRENDA database (Schomburg et al. 2017), the  
289 optimal temperature of GH11 xylanases (derived from several distinct microorganisms) varies from 22 to  
290 90 °C and the optimal pH from 2 to 11. However, most of these enzymes have an optimal activity between  
291 40 and 65 °C and pH 4-7. Therefore, the MetXyn11 activity profile is consistent with those of most of  
292 GH11 xylanases. Kinetics assays were performed under the enzyme optimal conditions, using  
293 glucuronoxylan as a substrate (Fig. 6C). Interestingly, the reactions revealed a “first-order reaction” profile  
294 even at 18 mg/L of substrate. Nevertheless, based on the data obtained predicted values of  $V_{max} = 50.30$   
295  $\mu M \cdot s^{-1}$ ,  $K_M$  of 121  $mg \cdot mL^{-1}$ ,  $k_{cat}$  of 1437  $s^{-1}$  and a catalytic efficiency ( $k_{cat}/K_M$ ) of 11.88  $mL \cdot s^{-1} \cdot mg^{-1}$ ,  
296 respectively, were obtained using GraphPad Prism 6.0 software (GraphPad Software Inc., La Jolla USA).  
297 The obtained  $K_M$  is consistent with a very poor binding of the enzyme to insoluble substrate  
298 (glucuronoxylan). A high  $K_M$  value offsets an elevated turnover number, resulting in a low catalytic  
299 efficiency of the enzyme on glucuronoxylan.

### 300 **Thermal and pH stability of MetXyn11**

301 MetXyn11 stability was evaluated both as a capacity to maintain the enzyme fold and a capacity  
302 to maintain its catalytic activity. For the former, we used Thermofluor analyses, in which MetXyn11 was  
303 exposed to a wide pH range during a linear increment on temperature until its thermal denaturation. The  
304 results show a signal from the fluorescence probe detected at the beginning of the experiment at pH 2,  
305 indicating enzyme denaturation (Fig. 5B). At pH 3, the MetXyn11 structure exhibited a low  $T_m$  value of 34  
306 °C, increasing to 44 °C at pH 4 until the maximum value of 52 °C at pH 6, and then discretely decreasing  
307 until 43 °C at pH 10 (Fig. 5B). Furthermore, residual activity of MetXyn11 was measured during 120 h  
308 under the optimal conditions for its enzymatic activity (Fig. 5C). MetXyn11 maintained almost 80% of its  
309 original activity after being incubated for 24 h, followed by 67%, 65%, 45% and 20%, respectively, after  
310 48 h, 72 h, 96 h and 120 h. MetXyn11 residual activity was also measured after 72 h at optimal temperature,  
311 but varying the pH from 2 to 10 (Fig. 5D). MetXyn11 presented no significant residual activity for pHs 2  
312 and 3. At pH 4, MetXyn11 retained 14% of its initial activity, about 70% at pH 5-6, 40% at pH 7, followed  
313 by a gradual decrease to 18% at pH 10.

### 314 **Enhancement of biomass hydrolysis by MetXyn11 supplementation to commercial enzymatic** 315 **cocktail**

316 To test the capacity of MetXyn11 to enhance biomass hydrolysis by a commercial enzymatic  
317 cocktail, we hydrolysed pretreated sugar cane bagasse using Cellic CTex3 alone and also supplemented by  
318 MetXyn3. Although MetXyn11 action alone did not lead to any detectable levels of released xylose or  
319 glucose, the enzyme addition to Cellic CTec3 led to a significantly enhanced hydrolytic activity of the  
320 cocktail on sugarcane bagasse as compared with the Cellic CTec3 alone. The levels of cellulose hydrolysis  
321 achieved in 24 h, 48 h, and 72 h, were 46.9%, 59.4%, and 63.3% respectively compared to Cellic CTec3  
322 alone, while they reached 54.5%, 67%, and 68.7% when Cellic CTec3 was combined with MetXyn11 (Fig.  
323 7A). Corroborating with the literature (Väljamäe et al. 1999; Boisset et al. 2001; Pellegrini et al. 2018), the  
324 relative increase in the hydrolysis yields was higher at the beginning of the reaction (at 24 h an increase in  
325 cellulose conversion was 16.6%) whereas at 48 h and 72 h the observed gains were 13.3%, and 8.6%. (Fig.  
326 7B). Levels of xylan hydrolysis, which reached 51.5%, 59.5% and 64% in 24 h, 48 h and 72 h using Cellic  
327 CTec3 alone, were increased to 53.9%, 62.2% and 66.7% when Cellic CTec3 was supplemented by

328 MetXyn11 (Fig. 7C&D). Thus, MetXyn11 addition provoked a significant increase of enzymatic hydrolysis  
329 of pretreated sugarcane bagasse when used in combination with Celic CTec3.

330

### 331 **Low resolution shape of MetXyn11 in solution**

332 SAXS studies were performed to determine the MetXyn11 low-resolution molecular envelope in  
333 solution. Structural parameters, data plot curves and the molecular envelope model obtained from SAXS  
334 experiments are summarized in Table S3 (Supplementary Materials), Figs. 8 and 9. Analysis of the initial  
335  $q$ -region of the scattering curves using Guinier approximation ( $\ln I(q)$  versus  $q^2$ ) exhibits the linear  
336 correlation expected for monodisperse samples, indicating homogeneity of the particles in solution (Fig.  
337 8A). In addition, the calculated  $R_g$  (18.52 Å) from each scattered frame remained constant (within the  
338 experimental errors) along the different protein concentrations, indicating: first, an absence of radiation  
339 damage and, second, an absence of attractive or repulsive interactions between the particles.

340 The distance-distribution  $p(r)$  plot has an almost perfect bell-shape, which is characteristic of well-  
341 defined spherical particles, but the curve also shows an extended tail with a small second peak at the highest  
342  $q$ -region (Fig. 8B), indicating that MetXyn11 might have a small module that protrudes from the overall  
343 globular shape (Perry and Tainer 2013). Moreover,  $D_{max}$  and  $R_g$  of MetXyn11 are equal to, respectively, 58  
344 Å and 17.67 Å, which is similar to the data obtained from Guinier analysis. The Porod-Debye plot ( $q^4 \times I(q)$   
345 versus  $q^4$ ) displays a clear plateau, which is consistent with the observation that MetXyn11 is a globular-  
346 like protein that lacks disordered regions (Fig. 8C) (Perry and Tainer 2013; De Oliveira et al. 2015; Rambo  
347 and Tainer 2011). The dimensionless Kratky curve ( $q^2 \times I(q)$  versus  $q$ ), which provides a notion about the  
348 degree of the particle compactness, has a well-defined maximum very close to 1.1 at  $qR_g = 1.6$ . That is,  
349 again, coherent with a nearly globular protein in solution (Fig. 8D) (Rambo and Tainer 2011; Perry and  
350 Tainer, 2013). Furthermore, at  $qR_g > 6$  there is a subtle elevated baseline, suggesting that MetXyn11 may  
351 exhibit some degree of flexibility (Perry and Tainer 2013; De Oliveira et al. 2015). All the experimental  
352 SAXS data fitted well to the theoretical SAXS plots generated from the 3D-homology model of MetXyn11  
353 structure. Finally, the low-resolution envelope snugly fits the 3D-homology model of the MetXyn11,  
354 revealing a monomeric globular-like protein with a protuberance at its N-terminus (Fig. 9).

355

## 356 **DISCUSSION**

### 357 **A novel GH11 xylosidase**

358 Substrate specificity assays using different plant polysaccharides revealed that MetXyn11  
359 exhibited activity only on glucuronoxyylan and arabinoxyylan. These results are in line with the previous  
360 observations since all known GH11 members are specific towards heteroxylans. Indeed, GH11 xylanases  
361 are considered to be “true”  $\beta$ -1,4-xylanases as compared to the other GH families (Pollet 2010; Paës et al.  
362 2012), which are frequently able to act on different polysaccharides in addition to heteroxylans. For  
363 example, there are known bifunctional xylanases from GH16, GH43 and GH62 that have two distinct  
364 catalytic domains, one with xylanase activity, while the other having glucanase activity (for GH16) or  
365 arabinase activity (for both GH43 and GH62) (Paës et al. 2012). Moreover, GH5, GH8, GH10, and GH30  
366 xylanases, which have a unique catalytic domain, show more versatility than members of the GH11 family.  
367 Some GH5 enzymes are specific for heteroxylans, however the GH5 family also includes cellulases,  
368 glucanases and mannanases (Pollet et al. 2010; Cantarel et al. 2009; Lombard et al. 2013). The same applies  
369 for the GH8 family, with a substitution of glucanases and mannanases for chitosanases and licheninases  
370 (Pollet et al. 2010; Cantarel et al. 2009; Lombard et al. 2013). The GH30 family contains both glucanases  
371 and galactanases (Cantarel et al. 2009; Lombard et al. 2013). Finally, the GH10 family mostly comprises  
372 endo- $\beta$ -1,4-xylanases, with a few examples of endo- $\beta$ -1,3-xylanases and  $\beta$ -1,4-xylosidases. Furthermore,  
373 GH10 enzymes can hydrolyze some glucose-derived substrates such as aryl-cello-oligosaccharides (Pollet  
374 et al. 2010).

375 The much lower activity of MetXyn11 towards arabinoxyylan as compared to glucuronoxyylan could  
376 be explained by a difference in the substrate’s decorations. Glucuronoxyylan used in our experiments is only  
377 ~13% decorated by glucuronic acid, while arabinoxyylan is ~40% decorated with arabinose residues. It is  
378 well known that GH11 xylanases have a narrow catalytic cleft unable to accommodate and cleave branched  
379 substrates (Pollet et al. 2010; Paës et al. 2012), which could explain MetXyn11 preference for  
380 glucuronoxyylan as compared to arabinoxyylan.

381 Quite remarkably though, despite having a profile of substrate specificity considered common  
382 among all GH11 endo- $\beta$ -1,4-xylanases, MetXyn11 revealed an uncommon pattern of hydrolytic products  
383 (Fig. 3 and Fig. 4). Typical GH11 endo- $\beta$ -1,4-xylanases release both xylobiose and xylotriose as main  
384 undecorated products from heteroxylans (Biely et al. 2016; Pollet et al. 2010). In addition, GH11 family

385 members also generate longer xylooligosaccharides (such as xylotetraose) linked to aldopentauronic acid  
386 or by L-arabinofuranosyl residue at the penultimate xylopyranosyl residue from the non-reducing end as  
387 their major decorated products released from glucuronoxylan and arabinoxylan, respectively (Biely et al.  
388 2016). In contrast, our HPAEC analyses identified xylobiose as the unique product released by MetXyn11  
389 both from glucuronoxylan and arabinoxylan, which is characteristic with its exo-catalytic activity (Fig. 3).  
390 Furthermore, our HPAEC results clearly show a conversion of xylohexaose into xylotetraose plus  
391 xylobiose, xylotetraose in xylobioses, and xylopentaose in xylotriose plus xylobiose. These results indicate  
392 that MetXyn11 cleaves off terminal xylobiose molecules from xylooligosaccharides and, also heteroxylans.

393 Our results are perfectly in line with the only other reported GH11 exo- $\beta$ -1,4-xylanase  
394 (Compost21\_GH11) (Mello et al. 2017). The Compost21\_GH11 hydrolysis of glucuronoxylan and  
395 xylooligosaccharides also revealed xylobiose as a unique product liberated by the enzyme. The crystal  
396 structure of Compost21\_GH11 (PDB: 5VQJ) has the typical  $\beta$ -jelly-roll fold shared by all the other 32  
397 GH11 xylanase structures deposited in PDB. However, Compost21\_GH11 has two extra loops not present  
398 in the other family members (Fig. 1B). These two extra loops are very close to the cleft and one of them  
399 clearly blocks part of the catalytic groove, evidencing its contribution for the uncommon exo-catalytic  
400 mechanism. Amino acid sequences alignment between MetXyn11 and Compost21\_GH11 (Fig. 1A)  
401 revealed that MetXyn11 also presents the two extra loops, which was also confirmed by the 3D  
402 superposition between the crystal structure of Compost21\_GH11 and the 3D-homology model of the  
403 MetXyn11 structure (Fig. 1C). Therefore, a MetXyn11 exo-catalytic mechanism could be mediated by the  
404 presence of these two extra loops.

405 Finally, our enzymatic kinetics results are consistent with the structural determinants of MetXyn11  
406 (Fig. 6). A typical narrow cleft of all GH11 family enzymes decorated with two uncommon extra loops  
407 (that might mediate MetXyn11 action as an exo-xylanase) significantly restrict MetXyn11 binding and  
408 recognition of heteroxylans. This could explain why MetXyn11 kinetics display a “first-order reaction”  
409 profile (as expected for very low concentrations of substrate binding-sites) even at high concentrations of  
410 glucuronoxylan.

#### 411 **Molecular shape of MetXyn11**

412 The analyses of amino acid sequence, SDS-PAGE, 3D-homology model and SAXS data provided  
413 important information about the size, shape, compactness, and flexibility of MetXyn11. These data show

414 that MetXyn11 is a monomeric globular-like enzyme of ~28 kDa, with a  $\beta$ -jelly-roll fold and a high degree  
415 of compactness,  $R_g$  between 17.6 and 18.5 Å and  $D_{max}$  close to 58 Å. These results are consistent with other  
416 GH11 xylanases from a wide diversity of microorganisms, as reviewed by Paës and collaborators on the  
417 basis of comparison of the biochemical and biophysical properties of 164 GH11 enzymes (Paës et al. 2012).  
418 This paper shows that xylanases uniquely formed by the catalytic module are dense globular proteins with  
419 molecular masses between 18 and 31 kDa, which have the same  $\beta$ -jelly-roll fold. Moreover, SAXS studies  
420 of a 21-kDa enzyme from *Trichoderma longibrachiatum* showed  $R_g$  and  $D_{max}$  close to 17 Å and 50 Å,  
421 respectively (Kozak 2006). As suggested by several authors, a relative small size and compactness of GH11  
422 xylanases facilitate their penetration into the inner part of PCW, consequently, indicating that these  
423 enzymes might initiate the PCW deconstruction, thus favoring consecutive action of larger enzymes (i.e  
424 multi-domains enzymes) (Paës et al. 2012; Beaugrand et al. 2005).

425 Despite having the  $\beta$ -jelly-roll fold (two twisted antiparallel  $\beta$ -sheets and a single  $\alpha$ -helix,  
426 resembling the shape of a partially closed right hand) that is traditional for all GH11 enzymes, our 3D-  
427 homology model and SAXS data revealed an unusual extra  $\alpha$ -helix at the MetXyn11 N-terminus, which is  
428 not present in all the 33 GH11 xylanases deposited in PDB, including the Compost21\_GH11. This  $\alpha$ -helix  
429 has a considerable degree of flexibility, as suggested by the Kratky plot, and promotes a clear protuberance  
430 at the N-terminal region of the MetXyn11 molecular envelope. The role of the additional  $\alpha$ -helix is not yet  
431 clear, thus requiring further experimental studies.

#### 432 **Possible biotechnological applications for MetXyn11**

433 As aluded to above, xylanases, especially those from GH10 and GH11 families, have a wide range  
434 of industrial applications (Polizeli et al. 2005; Kalim et al. 2015; Biely et al. 2016). The ability of  
435 MetXyn11 to liberate xylobiose as the only soluble product might be advantageous for pre- and pro-  
436 biotic formulations. Xylo-oligosaccharides find applications in the food sector due to their health benefits  
437 and some biochemical characteristics which are considered advantageous when compared to other oligo-  
438 saccharides. For example, xylo-oligosaccharides are stable over a wide pH range (2.5-8.0) and also at  
439 temperatures up to 100 °C, in contrast to others non-digestible oligosaccharides such as fructo-  
440 oligosaccharides, for example, that are unstable at the human gastric acid pH (Vazquez et al. 2000; Kumar  
441 et al. 2012). Furthermore, xylobiose has a higher antifreeze activity than glucose, sucrose and maltose, and  
442 also has a water activity similar to that shown by glucose (Vazquez et al. 2000; Kumar et al. 2012). Besides,

443 xylobiose is not carcinogenic, has acceptable odor and low calories, which favors its use in diet products  
444 formulation (Vazquez et al. 2000; Kumar et al. 2012).

445 In addition, MetXyn11 has the highest specific activity around 50 °C, and also presents good  
446 stability at this temperature for 72 h or longer. These are important enzymatic properties for industrial  
447 applications, since temperatures close or above 50 °C are usually required in the processing of complex  
448 polysaccharides to reduce its high viscosity and also help to prevent the undesirable growth of mesophilic  
449 contaminants (Kozak 2006). Moreover, MetXyn11 has a wide pH range of activity (pH 5-10),  
450 demonstrating high stability (70%) between pHs 5 and 6 after 72 h at 50 °C. These results suggest that  
451 MetXyn11 could be used both in the processes that require alkaline pHs (i.e pulp and paper biobleaching)  
452 (Walia et al. 2017) and also in the processes which need acid pHs (i.e fruit juice and wine preparation)  
453 (Beaugrand et al. 2005).

454 Finally, MetXyn11 could be used as a complement of commercial enzymatic cocktails aiming for  
455 better yields of plant biomass enzymatic hydrolysis, as demonstrated by our Cellic CTec3 complementation  
456 experiments. MetXyn11 supplementation not only enhances levels of xylan hydrolysis, but also  
457 considerably increases levels of cellulose hydrolysis by Cellic CTec3 cellulases (Fig. 7). It is known that  
458 that Cellic CTec3 has endo- $\beta$ -1,4-xylanase and  $\beta$ -xylosidase activities (Sun et al 2015; Hu et al 2016). It  
459 may be expected that xylobiose generated by the exo-xylanase is hydrolyzed into xylan as well as that  
460 primary sugarcane bagasse xylan hydrolysis products generated by the xylanase activity of Cellic CTec3  
461 are subsequently shortened by exo-xylanase activity of MetXyn11, resulting in the enhance of  
462 hemicellulose hydrolysis. It was shown that the xylan polymer can bind tightly to the hydrophilic surfaces  
463 of the cellulose crystallites  $2_1$ -fold helical screw conformation within the plant cell wall, thus significantly  
464 interfering with the cellulose enzymatic hydrolysis (Busse-Wicher et al 2014). Furthermore, pretreatment  
465 solubilized hemicellulose oligomers partly aggregate on the cellulose surfaces and physically block access  
466 of cellulases on the cellulose fibres (Kabel et al. 2007; Kumar et al. 2018). Moreover, solubilized fragments  
467 of the xylan backbone (xylooligosaccharides, XOS) and mixed-linkage  $\beta$ -glucans are strong inhibitors of  
468 cellulases (Kont et al 2013). Therefore, it was shown that  $\beta$ -xylanase supplementation increases cellulose  
469 hydrolysis in xylan-containing lignocellulosic materials (Zhang et al. 2011; Kont et al 2013; Sun et al 2015;  
470 Kumar et al 2018). Here we demonstrated that MetXyn11 supplementation of Cellic CTec3 leads to a  
471 significant increase in rates and yields of cellulose and xylan conversion from pretreated lignocellulosic  
472 biomass.

473 **Final considerations: MetXyn11 is an unusual GH11  $\beta$ -1,4-xylosidase**

474 Our current work supports an importance of metatranscriptomic approaches for discovering novel  
475 and unusual enzymes that are not accessible by the traditional approaches of microbial cultivation in pure  
476 cultures, as so far, MetXyn11 is the second reported GH11 enzyme with a  $\text{exo-}\beta$ -1,4-catalytic mechanism.  
477 Homology modeling and amino acid sequence comparison indicate that the same two extra loops already  
478 described for the first reported GH11  $\text{exo-}\beta$ -1,4-xylanase (Compost21\_GH11) are also present in  
479 MetXyn11. In addition, MetXyn11 has an extra N-terminus  $\alpha$ -helix which does not exist in other GH11  
480 enzymes deposited in PDB, including the Compost21\_GH11. Our results also reveal that MetXyn11 is a  
481 monomeric globular-like enzyme with biochemical properties that could be attractive for biotechnological  
482 applications, such as: high substrate specificity; wide pH range of activity (pH 5-10) and high pH stability  
483 at pH 5-6 (at optimum temperature); high thermal stability at 50 °C (at optimum pH) for long periods of  
484 time; and a unique hydrolytic product release pattern. Indeed, the enzyme exclusively produces xylobiose,  
485 which is considered an added-value molecule for various applications. Furthermore, the enzyme addition  
486 provoked considerable increase in Cellic CTec3 hydrolysis yields of pretreated sugar cane bagasse, which  
487 could be of interest for second generation bioethanol production.

488 **FUNDING**

489 This study was supported by the Fundação de Amparo à Pesquisa do Estado de São Paulo  
490 (FAPESP) via grants #10/52362-5, 11/20505-4, 11/21608-1 and 15/13684-0, the Conselho Nacional de  
491 Desenvolvimento Científico e Tecnológico (CNPq) via grants # 405191/2015-4, 303988/2016-9,  
492 440977/2016-9 and 151963/2018-5 and the BBSRC of the UK Research and Innovation (grant number:  
493 BB/I018492/1).

494 **AUTHORS CONTRIBUTIONS**

495 I.P and D.E.E designed the experiments and wrote the manuscript. D.E.E and V.O.A.P performed  
496 MetXyn11 biochemical and biophysical characterization. D.E.E performed the SAXS experiments. M.E.S  
497 provided pretreated bagasse samples. I.P., S.M.M., N.C.B., D.E.E. and V.O.A.P. contributed to discussion  
498 of the results and editing of the manuscript. All the authors approved the final version.

499 **CONFLICT OF INTEREST**

500 The authors declare that they have no conflict of interest.

## 501 COMPLIANCE WITH ETHICAL STANDARDS AND ETHICAL APPROVAL

502 This article does not contain any studies with human or animal participants.

## 503 REFERENCES

- 504 Altschul SF, Gish W, Miller W, Myers EW, Lipman DJ (1990) Basic local alignment search tool. *J Mol Biol* 215:403-410. doi: 10.1016/S0022-2836(05)80360-2
- 506 Beaugrand J, Paës G, Reis D, Takahashi M, Debeire P, O'Donoghue M, Chabbert B (2005) Probing the  
507 cell wall heterogeneity of micro-dissected wheat caryopsis using both active and inactive forms  
508 of a GH11 xylanase. *Planta* 222:246-257. doi: 10.1007/s00425-005-1538-0
- 509 Biely P, Singh S, Puchart V (2016) Towards enzymatic breakdown of complex plant xylan structures:  
510 State of the art. *Biotechnol Adv* 34:1260–1274. doi: 10.1016/j.biotechadv.2016.09.001
- 511 Boisset C, Pétrequin C, Chanzy H, Henrissat B, Schüleïn M (2001) Optimized mixtures of recombinant  
512 *Humicola insolens* cellulases for the biodegradation of crystalline cellulose. *Biotechnol Bioeng*  
513 72:339-345. doi: 10.1002/1097-0290(20010205)72:3<339::AID-BIT11>3.0.CO;2-%23
- 514 Camilo C, Polikarpov I (2014) High-throughput cloning, expression and purification of glycoside  
515 hydrolases using ligation-independent cloning (LIC). *Protein Expr Purif* 99:35-42. doi:  
516 10.1016/j.pep.2014.03.008
- 517 Cantarel BL, Coutinho PM, Rancurel C, Bernard T, Lombard V, Henrissat B (2009) The Carbohydrate-  
518 Active EnZymes database (CAZy): an expert resource for glycogenomics. *Nucleic Acids Res* 37:  
519 D233-D238. doi: 10.1093/nar/gkn663.
- 520 Castillo JM, Romero E, Nogales, R (2013) Dynamics of microbial communities related to biochemical  
521 parameters during vermicomposting and maturation of agroindustrial lignocellulose wastes.  
522 *Bioresour Technol* 146:345-354. doi: 10.1016/j.biortech.2013.07.093
- 523 Curtis TP, Head IM, Graham DW (2003) Theoretical ecology for engineering biology. *Environ Sci*  
524 *Technol* 37:64A-70A. doi: 10.1021/es0323493
- 525 DeLano WL (2002) The PyMOL Molecular Graphics System. Palo Alto, CA, USA.: DeLano Scientific.  
526 <http://www.pymol.org>.
- 527 de Oliveira LC, da Silva VM, Colussi F, Cabral AD, de Oliveira Neto M, Squina FM, Garcia W (2015)  
528 Conformational changes in a hyperthermostable glycoside hydrolase: enzymatic activity is a  
529 consequence of the loop dynamics and protonation balance. *PLoS One* 10: e0118225. doi:  
530 10.1371/journal.pone.0118225
- 531 Duan CJ, Feng JX (2010) Mining metagenomes for novel cellulase genes. *Biotechnol Lett* 32: 1765-1775.  
532 doi: 10.1007/s10529-010-0356-z
- 533 Ericsson UB, Hallberg BM, Detitta GT, Dekker N, Nordlund P (2006) Thermofluor-based high-  
534 throughput stability optimization of proteins for structural studies. *Anal Biochem* 357:289-98.  
535 doi: 10.1016/j.ab.2006.07.027
- 536 Evangelista DE, de Paula FF, Rodrigues A, Henrique-Silva F (2015) Pectinases from *Sphenophorus levis*  
537 Vaurie, 1978 (Coleoptera: *Curculionidae*): Putative accessory digestive enzymes. *J Insect Sci*  
538 15:1536-2442. doi: 10.1093/jisesa/ieu168
- 539 Evangelista DE, Kadowaki MAS, Mello BL, Polikarpov I (2018) Biochemical and biophysical  
540 characterization of novel GH10 xylanase prospected from a sugar cane bagasse compost-derived  
541 microbial consortia. *Int J Biol Macromol* 109:560-568. doi: 10.1016/j.ijbiomac.2017.12.099

- 542 Franke D, Svergun D (2009) DAMMIF, a program for rapid ab-initio shape determination in small-angle  
543 scattering. *J Appl Crystallogr* 42:342-346. doi: 10.1107/S0021889809000338
- 544 Ghio S, Ontañón O, Piccinni FE, Díaz de Villegas RM, Talia P, Grasso DH, Campos E (2018)  
545 *Paenibacillus* sp. A59 GH10 and GH11 extracellular endoxylanases: Application in biomass  
546 bioconversion. *BioEnergy Research* 11:174–190. doi: 10.1007/s12155-017-9887-7
- 547 Guinier A, Fournet G, Walker CB (1995) Small angle scattering of X-rays. *Phys Today* 9:38-9
- 548 Hu J, Davies J, Mok YK, Gene B, Lee QF, Arato C, Saddler JN (2016) Enzymatic hydrolysis of industrial  
549 derived xylo-oligomers to monomeric sugars for potential chemical/biofuel production. *ACS*  
550 *Sustain Chem Eng* 4: 7130-7136. doi: 10.1021/acssuschemeng.6b02008
- 551 Isikgor F, Becer C (2015) Lignocellulosic biomass: a sustainable platform for the production of bio-based  
552 chemicals and polymers. *Polymer Chem* 6: 4497-4559. doi: 10.1039/C5PY00263J
- 553 Johansson K, El-Ahmad M, Friemann R, Jörnvall H, Markovic O, Eklund H (2002) Crystal structure of  
554 plant pectin methylesterase. *FEBS Lett* 514:243-249. doi: 10.1016/S0014-5793(02)02372-4
- 555 Johnson E (2016) Integrated enzyme production lowers the cost of cellulosic ethanol. *Biofuels Bioprod*  
556 *Bioref* 10:164-174. doi:10.1002/bbb.1634
- 557 Kabel MA, den Borne H, Vincken JP, Voragen AGJ, Schols HA (2007) Structural differences of xylans  
558 affect their interaction with cellulose. *Carbohydrate Polym* 69:94-105. doi:  
559 10.1016/j.carbpol.2006.09.006
- 560 Kalim B, Böhringer N, Ali N, Schäberle TF (2015) Xylanases—from microbial origin to industrial  
561 application. *British Biotechnol J* 7:1-20. doi: 10.9734/BBJ/2015/15982
- 562 Keegstra K (2010) Plant cell walls. *Plant Physiol* 154:483-486. doi: 10.1104/pp.110.161240
- 563 Konarev P, Svergun D (2015) A posteriori determination of the useful data range for small-angle  
564 scattering experiments on dilute monodisperse systems. *IUCrJ* 2:352-360. doi:  
565 10.1107/S2052252515005163
- 566 Kont R, Kurašin M, Teugjas H, Väljamäe, P (2013) Strong cellulase inhibitors from the hydrothermal  
567 pretreatment of wheat straw. *Biotechnol Biofuels* 6:135. doi:10.1186/1754-6834-6-135
- 568 Kozak M (2006) Solution scattering studies of conformation stability of xylanase XYNII from  
569 *Trichoderma longibrachiatum*. *Biopolymers* 83:95-102. doi: 10.1002/bip.20531
- 570 Kozin M, Svergun D (2001) Automated matching of high- and low-resolution structural models. *J Appl*  
571 *Crystallogr* 34: 33-41. doi: 10.1107/S0021889800014126
- 572 Kumar G, Pushpa A, Prabha H (2012) A review on xylooligosaccharides. *Int Res J Pharm* 3:71-74.
- 573 Kumar R, Bhagia S, Smith MD, Petridis L, Ong RG, Cai CM, Mittal A, Himmel MH, Balan V, Dale  
574 BE, Ragauskas AJ, Smith JC, Wyman CE (2018) Cellulose–hemicellulose interactions at  
575 elevated temperatures increase cellulose recalcitrance to biological conversion. *Green Chem* 20:  
576 921–934. doi: 10.1039/c7gc03518g
- 577 Liao H, Zheng H, Li S, Wei Z, Mei X, Ma H, Shen Q, Xu Y (2015) Functional diversity and properties of  
578 multiple xylanases from *Penicillium oxalicum* GZ-2. *Sci Rep* 5:12631. doi: 10.1038/srep12631.
- 579 Lombard V, Golaconda RH, Drula E, Coutinho PM, Henrissat B (2014) The carbohydrate-active enzymes  
580 database (CAZy) in 2013. *Nucleic Acids Res* 42: D490-D495. doi: 10.1093/nar/gkt1178.
- 581 Mello BL, Alessi AM, McQueen-Mason S, Bruce NC, Polikarpov I (2016) Nutrient availability shapes  
582 the microbial community structure in sugarcane bagasse compost-derived consortia. *Sci Rep*  
583 6:38781. doi: 10.1038/srep38781

- 584 Mello BL, Alessi AM, Riaño-Pachón DM, deAzevedo ER, Guimarães FEG, Espírito-Santo MC,  
585 McQueen-Mason S, Bruce NC, Polikarpov I (2017) Targeted metatranscriptomics of compost-  
586 derived consortia reveals a GH11 exerting an unusual exo-1,4- $\beta$ -xylanase activity. *Biotechnol*  
587 *Biofuels* 10:254. doi: 10.1186/s13068-017-0944-4
- 588 Miller GL (1959) Use of dinitrosalicylic acid reagent for determination of reducing sugar. *Anal Chem*  
589 31:426-428
- 590 Notredame C, Higgins DG, Heringa J (2000) T-coffee: a novel method for fast and accurate multiple  
591 sequence alignment. *J Mol Biol* 302:205-217. doi: 10.1006/jmbi.2000.4042
- 592 Paës G, Berrin JG, Beaugrand J (2012) GH11 xylanases: Structure/function/properties relationships and  
593 applications. *Biotechnol Adv* 30:564-592. doi:10.1016/j.biotechadv.2011.10.003
- 594 Pauchet Y, Wilkinson P, Chauhan R, French-Constant RH (2010) Diversity of beetle genes encoding  
595 novel plant cell wall degrading enzymes. *PLoS One* 5:e15635. doi:  
596 10.1371/journal.pone.0015635.
- 597 Pellegrini VOA, Bernardes A, Rezende CA, Polikarpov I (2018) Cellulose fiber size defines efficiency of  
598 enzymatic hydrolysis and impacts degree of synergy between endo- and exoglucanases.  
599 *Cellulose* 25:1865-1881. doi:10.1007/s10570-018-1700-z
- 600 Petersen TN, Brunak S, von Heijne G, Nielsen H (2011) SignalP 4.0: discriminating signal peptides from  
601 transmembrane regions. *Nat Methods* 8:785-786. doi: 10.1038/nmeth.1701
- 602 Perry J, Tainer J (2013) Developing advanced X-ray scattering methods combined with crystallography  
603 and computation. *Methods* 59:363-371. doi: 10.1016/j.ymeth.2013.01.005
- 604 Pollet A, Delcour JA, Courtin CM (2010) Structural determinants of the substrate specificities of  
605 xylanases from different glycoside hydrolase families. *Crit Rev Biotechnol* 30:176-191. doi:  
606 10.3109/07388551003645599
- 607 Polizeli ML, Rizzatti AC, Monti R, Terenzi HF, Jorge JA, Amorim DS (2005) Xylanases from fungi:  
608 properties and industrial applications. *Appl Microbiol Biotechnol* 67:577-591. doi:  
609 10.1007/s00253-005-1904-7
- 610 Rambo RP, Tainer JA (2011) Characterizing flexible and intrinsically unstructured biological  
611 macromolecules by SAS using the Porod-Debye law. *Biopolymers* 95:559-571. doi:  
612 10.1002/bip.21638
- 613 Rittmann BE, Hausner M, Löffler F, Love NG, Muyzer G, Okabe S, Oerther DB, Peccia J, Raskin L,  
614 Wagner M (2006) A vista for microbial ecology and environmental biotechnology. *Environ Sci*  
615 *Technol* 40:1096-103. doi: 10.1021/es062631k
- 616 Santo ME, Rezende CA, Bernardinelli OD, Pereira N, Curvelo AAS, Deazevedo ER, Guimarães  
617 FEG, Polikarpov I (2018) Structural and compositional changes in sugarcane bagasse subjected  
618 to hydrothermal and organosolv pretreatments and their impacts on enzymatic hydrolysis. *Ind*  
619 *Crop Prod* 113:64-74. doi: 10.1016/j.indcrop.2018.01.014
- 620 Schomburg I, Jeske L, Ulbrich M, Placzek S, Chang A, Schomburg D (2017) The BRENDA enzyme  
621 information system-From a database to an expert system. *J Biotechnol* 261:194-206. doi:  
622 10.1016/j.jbiotec.2017.04.020
- 623 Shi P, Du Y, Yang H, Huang H, Zhang X, Wang Y, Yao B (2015) Molecular characterization of a new  
624 alkaline-tolerant xylanase from *Humicola insolens* Y1. *Biomed Res Int* 2015:149504. doi:  
625 10.1155/2015/149504
- 626 Silva COG, Vaz RP, Filho EXF (2018) Bringing plant cell wall degrading enzymes into the  
627 lignocellulosic biorefinery concept. *Biofuels Bioprod Bioref* 12:277-289. doi:  
628 10.1002/bbb.1832

629 Sims RE, Mabee W, Saddler JN, Taylor M (2010) An overview of second generation biofuel  
630 technologies. *Bioresour Technol* 101:1570-1580. doi: 10.1016/j.biortech.2009.11.046

631 Slabinski L, Jaroszewski L, Rychlewski L, Wilson IA, Lesley SA, Godzik A (2007) XtalPred: a web  
632 server for prediction of protein crystallizability. *Bioinform* 23:3403-3405. doi:  
633 10.1093/bioinformatics/btm477

634 Sun FF, Hong J, Hu J, Saddler JN, Fang X, Zhang Z, Shen S (2015) Accessory enzymes influence  
635 cellulase hydrolysis of the model substrate and the realistic lignocellulosic biomass. *Enzyme  
636 Microbial Technol* 79:42–48. doi: 10.1016/j.enzmictec.2015.06.020

637 Suzuki M, Kato A, Nagata N, Komeda Y (2002) A xylanase, AtXyn1, is predominantly expressed in  
638 vascular bundles, and four putative xylanase genes were identified in the *Arabidopsis thaliana*  
639 genome. *Plant Cell Physiol* 43:759-767. doi: 10.1093/pcp/pcf088

640 Svergun DI (1992) Determination of the regularization parameter in indirect-transform methods using  
641 perceptual criteria. *J Appl Crystallogr* 25:495-503. doi: 10.1107/S0021889892001663

642 Svergun DI, Barberato C, Koch M (1995) CRY SOL - A program to evaluate x-ray solution scattering of  
643 biological macromolecules from atomic coordinates. *J Appl Crystallogr* 28:768-773. doi:  
644 10.1107/S0021889895007047

645 Våljamäe P, Sild V, Nutt A, Pettersson G, Johansson G (1999) Acid hydrolysis of bacterial cellulose  
646 reveals different modes of synergistic action between cellobiohydrolase I and endoglucanase I.  
647 *Eur J Biochem* 266:327-334. doi: 10.1046/j.1432-1327.1999.00853.x

648 Vázquez MJ, Alonso JL, Domínguez H, Parajó JC (2000). Xylooligosaccharides: manufacture and  
649 applications. *Trends Food Sci Technol* 11:387-393. doi: 10.1016/S0924-2244(01)00031-0

650 Volkov V, Svergun D (2003) Uniqueness of ab initio shape determination in small-angle scattering. *J  
651 Appl Crystallogr* 36:860-864. doi: 10.1107/S0021889803000268

652 Walia A, Guleria S, Mehta P, Chauhan A, Parkash J (2017) Microbial xylanases and their industrial  
653 application in pulp and paper biobleaching: a review. *3 Biotech* 7:11-22. doi: 10.1007/s13205-  
654 016-0584-6

655 Watanabe H, Tokuda G (2001) Animal cellulases. *Cell Mol Life Sci* 58:1167-78. doi:  
656 10.1007/PL00000931

657 Wilkins M, Gasteiger E, Bairoch AM, Sanchez JE, Williams K, Appel RD, Hochstrasser D (1999) Protein  
658 identification and analysis tools in the ExPASy server. *Methods Mol Biol* 112:531-552

659 Yang J, Yan R, Roy A, Xu D, Poisson J, Zhang Y (2015) The I-TASSER Suite: protein structure and  
660 function prediction. *Nat Methods* 12:7-8. doi:10.1038/nmeth.3213

661 Zhang J, Tuomainen P, Siika-aho M, Viikari L (2011) Comparison of the synergistic action of two  
662 thermostable xylanases from GH families 10 and 11 with thermostable cellulases in  
663 lignocellulose hydrolysis. *Bioresour Technol* 102: 9090-9095. doi:  
664 10.1016/j.biortech.2011.06.085

665 Zhou J, Shi P, Zhang R, Huang H, Meng K, Yang P, Yao B (2011) Symbiotic *Streptomyces sp.* TN119  
666 GH 11 xylanase: a new pH-stable, protease- and SDS-resistant xylanase. *J Ind Microbiol  
667 Biotechnol* 38:523-530. doi: 10.1007/s10295-010-0795-5

668

669

670

671 **Figure Captions**

672 **Fig. 1: Sequences and structures of selected GH11 enzymes.** (A) Multiple alignment between the amino  
673 acid sequences from MetXyn11, Compost21\_GH11 (PDB id: 5VQJ), and several typical GH11 endo-1,4-  
674  $\beta$ -xylanases (PDB ids: 1XNK, 1H1A, 1XYP, 2JIC and 4XQD). The yellow box shows the extended amino  
675 acid sequence present exclusively at the N-terminal of MetXyn11, the red boxes show the two extra loops  
676 existent only in MetXyn11 and Compost21\_GH11 exo-1,4- $\beta$ -xylanases. (B) Multiple superposition of the  
677 Compost21\_GH11 and typical GH11 endo-1,4- $\beta$ -xylanases crystallographic structures. (C) Superposition  
678 of the MetXyn11 3D homology model and the Compost21\_GH11 crystallographic structure.

679 **Fig. 2: Expression and purification of Xyn11.** SDS-PAGE shows MetXyn11 purification steps; M:  
680 molecular mass marker; 0: total soluble protein after IPTG induction; 1: Xyn11 attached to 6xHis-tag, after  
681 the first  $\text{Ni}^{+2}$  affinity chromatography; 2: Xyn11 devoid the fusion 6xHis-tag after the second  $\text{Ni}^{+2}$  affinity  
682 chromatography; 3: final purified Xyn11 after size exclusion chromatography. Size exclusion molecular  
683 chromatography shows a unique peak of elution, confirming the sample purity.

684 **Fig. 3: Cleavage pattern of MetXyn11 on heteroxylans.** The cleavage pattern of MetXyn11 was assessed  
685 and compared with the cleavage pattern from a typical GH11 endo-1,4- $\beta$ -xylanase (rGH11XynB).  
686 Reactions were performed under the optimal conditions of enzymes for 24 h, using glucuronoxylan and  
687 arabinoxylan as substrates. The generated soluble products were analyzed by HPAEC-PAD. (A) and (D):  
688 Standards: Solution containing xylooligosaccharides (XOS) from xylose ( $\text{X}_1$ ) to xylohexaose ( $\text{X}_6$ ). (B)  
689 Reaction products of rGH11XynB action on glucuronoxylan. (C) Reaction products of MeTXyn11 action  
690 on glucuronoxylan. (E) Reaction products of rGH11XynB action on arabinoxylan. (F) Reaction products  
691 of MeTXyn11 action on arabinoxylan. The results showed a clear difference between the cleavage patterns  
692 of MetXyn11 and rGH11XynB. MetXyn11 releases xylobiose as the only product from both substrates,  
693 whereas rGH11XynB generates several other xylooligosaccharides in addition to xylobiose. The results  
694 also showed the preference of MetXyn11 for less decorated heteroxylans, since the enzyme liberated much  
695 more xylobiose from glucuronoxylan (13% decorated) than arabinoxylan (40% decorated).

696 **Fig. 4: Cleavage pattern of MetXyn11 on xylooligosaccharides.** The MetXyn11 mechanism of action on  
697 homoxylan was assessed by HPAEC-PAD analysis, using xylohexaose as a model substrate. Reactions  
698 were conducted under the enzyme optimal conditions for 1, 5, 10 and 15 min. A profile of released  
699 xylooligosaccharides observed over a period of 15 min shows conversion of xylohexaose in xylotetraose  
700 plus xylobiose, and xylotetraose in two xylobioses, besides the conversion of xylopentaose in xylotriose  
701 plus xylobiose. Therefore, MetXyn11 cleaves and liberates xylobiose as the only product which is  
702 consistent with an exo-catalytic mechanism of the enzyme.

703 **Fig. 5: Thermal and pH stability of MetXyn11.** The thermal stability of MetXyn11 was assessed by both  
704 Thermofluor (A-B) and residual activity assays (C-D). In Thermofluor assay, MeTXyn11 was exposed to  
705 a wide pH range during a linear increase in temperature until protein thermal denaturation. (A) At the  
706 optimal buffer condition (potassium phosphate pH 7.0) MetXyn11 has a  $T_m$  of 55 °C. (B) MetXyn11 has  
707 excellent pH stability in a wide range from pH 4 to 10 in ABF buffer. For residual activity assay, MetXyn11  
708 activity was measured after keeping the enzyme for 120 h under the optimal conditions for its activity and

709 also measured after 72 h at optimal temperature (50 °C), but varying pH from 2 to 10. (C) The enzyme has  
710 good thermostability, maintaining 45% of its original activity after 96 h of incubation. (D) MetXyn11 also  
711 has good pH stability at pH 5-6 (above 70%).

712 **Fig. 6: Optimal activity conditions and kinetics of MetXyn11.** The optimum pH was evaluated in pH  
713 range from 2 to 10 in ABF buffer at 50 °C, while the optimal temperature was assessed in a potassium  
714 phosphate buffer at pH 7.0, varying temperature of the experiment from 30 to 70 °C. MetXyn11 has the  
715 highest activity around 50 °C (A) and pH 6-7 (B). Kinetics experiments revealed a “first-order reaction”  
716 profile for MetXyn11 catalytic action even at a high substrate concentration. Kinetic parameters obtained  
717 by fitting of this curve resulted in the values of 50.30  $\mu\text{M}\cdot\text{s}^{-1}$ , 121  $\text{mg}\cdot\text{mL}^{-1}$ , 1437  $\text{s}^{-1}$  and 11.88  $\text{mL}\cdot\text{s}^{-1}\cdot\text{mg}^{-1}$   
718 for  $V_{\text{max}}$ ,  $K_M$ ,  $k_{\text{cat}}$  and  $k_{\text{cat}}\cdot K_M^{-1}$ , respectively.

719 **Fig. 7: Yields of enzymatic hydrolysis of pretreated sugarcane bagasse.** Enhancement of commercial  
720 enzymatic cocktail Celic CTec3 by addition of MetXyn11 was assessed by HPLC analyses of glucose and  
721 xylose under optimal CTec3 conditions of pH and temperature, using hydrothermal pretreated sugarcane  
722 bagasse as a substrate. (A) Yield of glucose release as a function of the time using Celic CTec3 alone, and  
723 using a mixture of Celic CTec3 plus MetXyn11. (B) The relative increments in the yields of released  
724 glucose as a function of the time. (C) Yield of xylose release as a function of the time using Celic CTec3  
725 alone and using a mixture of Celic CTec3 plus MetXyn11. (D) The relative increments in the yields of  
726 released xylose as a function of the time.

727 **Fig. 8: SAXS analysis.** (A) Experimental solution scattering profile superimposed with the theoretical  
728 scattering profile calculated based on MetXyn11 3D homology model. The insert figure shows that the  
729 Guinier plot data and the linear regression satisfy the approximation  $q < 1.3/R_g$ . (B) The  $p(r)$  plot displays  
730 an almost perfect bell-shape, including an extended tail with a small second peak at the highest  $q$ -region,  
731 indicating a small deviation of ellipsoidal shape. (C) Porod-Debye plot displays a clear plateau, expected  
732 for globular-like proteins that lack disordered regions. (D) The dimensionless Kratky plot presents a well-  
733 defined maximum that is consistent with a globular protein, and also presents a subtle elevated baseline at  
734  $qR_g > 6$ , suggesting some flexibility of the protein structure.

735 **Fig. 9: MetXyn11 low-resolution molecular envelope computed from experimental SAXS data.** The  
736 3D-homology model of MetXyn11 (colored) was superposed into the average ab initio SAXS envelope  
737 (gray). The N-terminus (N-term) and C-terminus (C-term) of MetXyn11 are indicated for better orientation.  
738 The low-resolution envelope fits well the 3D homology model of MetXyn11, revealing a monomeric  
739 globular-like protein with a protuberance at its N-terminus.

740

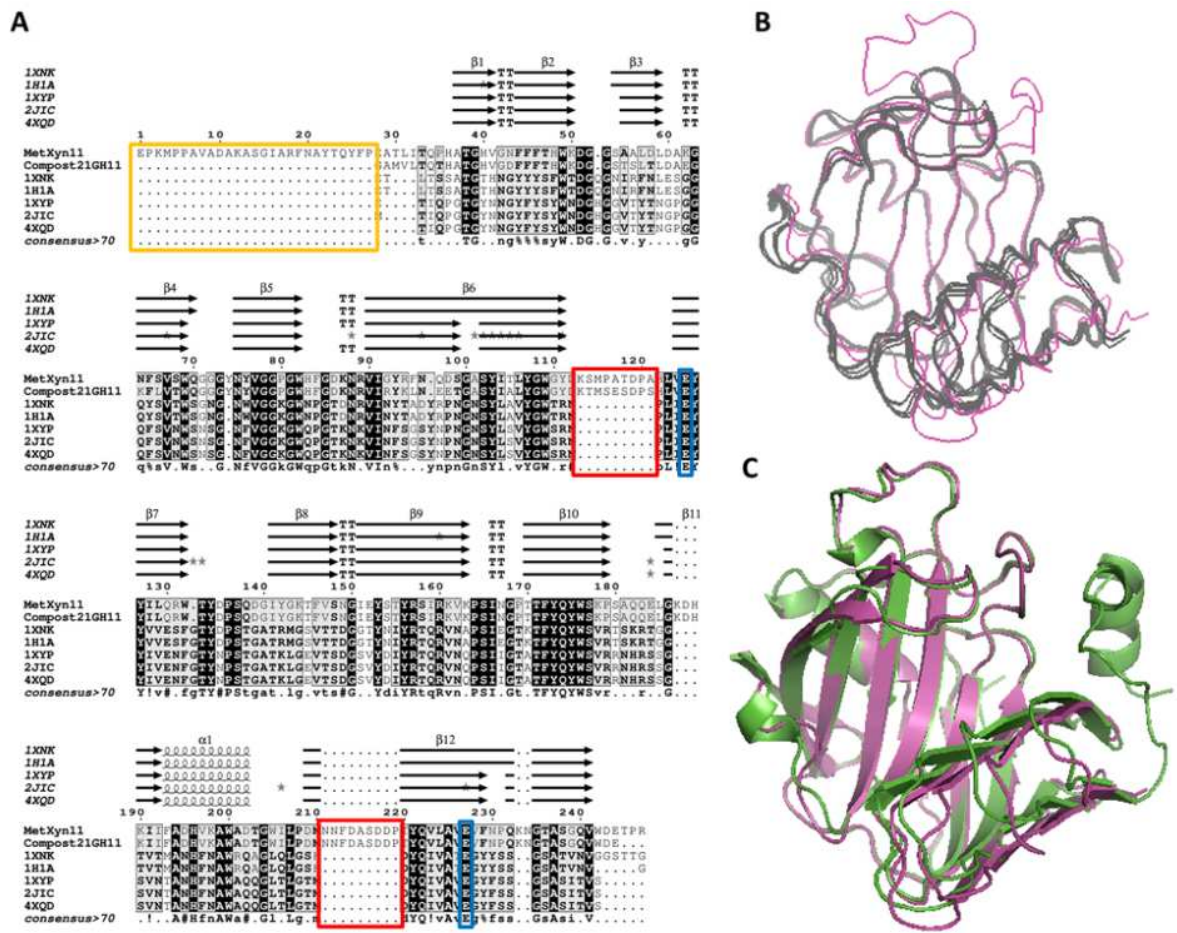


**Fig. 1: Sequences and structures of selected GH11 enzymes.** (A) Multiple alignment between the amino acid sequences from MetXyn11, Compost21\_GH11 (PDB id: 5VQJ), and several typical GH11 endo-1,4-674  $\beta$ -xylanases (PDB ids: 1XNK, 1H1A, 1XYP, 2JIC and 4XQD). The yellow box shows the extended amino acid sequence present exclusively at the N-terminal of MetXyn11, the red boxes show the two extra loops existing only in MetXyn11 and Compost21\_GH11 exo-1,4- $\beta$ -xylanases. (B) Multiple superposition of the Compost21\_GH11 and typical GH11 endo-1,4- $\beta$ -xylanases crystallographic structures. (C) Superposition of the MetXyn11 3D homology model and the Compost21\_GH11 crystallographic structure.

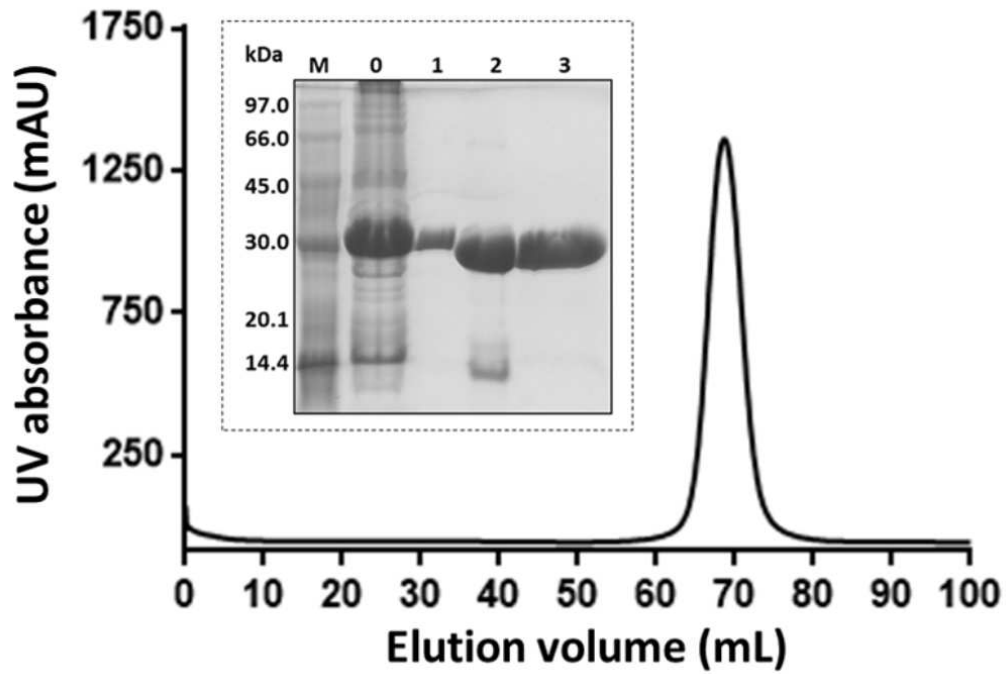


**Fig. 2: Expression and purification of Xyn11.** SDS-PAGE shows MetXyn11 purification steps; M: molecular mass marker; 0: total soluble protein after IPTG induction; 1: Xyn11 attached to 6xHis-tag, after the first  $\text{Ni}^{+2}$  affinity chromatography; 2: Xyn11 devoid of the fusion 6xHis-tag after the second  $\text{Ni}^{+2}$  affinity chromatography; 3: final purified Xyn11 after size exclusion chromatography. Size exclusion chromatography shows a unique peak of elution, confirming the sample purity.

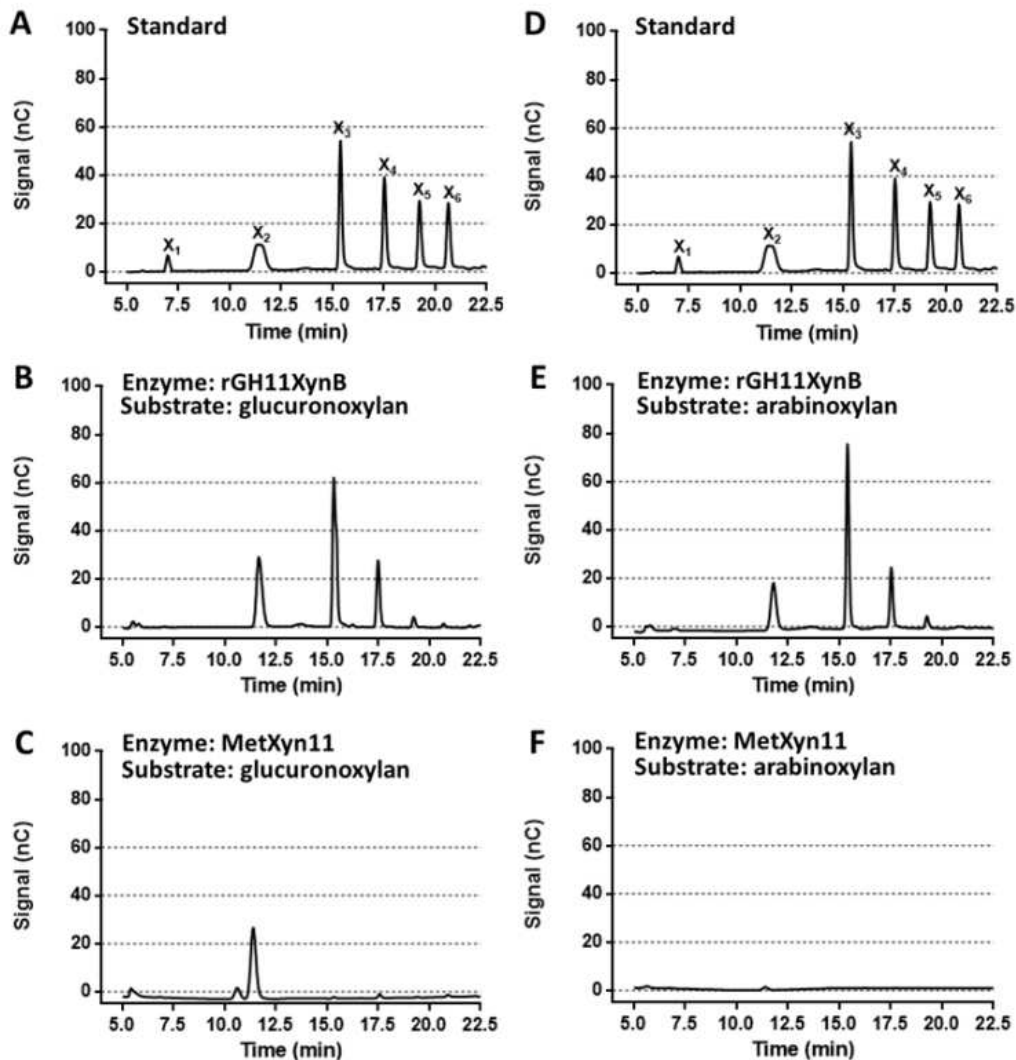


**Fig. 3: Cleavage pattern of MetXyn11 on heteroxylans.** The cleavage pattern of MetXyn11 was assessed and compared with the cleavage pattern from a typical GH11 endo-1,4- $\beta$ -xylanase (rGH11XynB). Reactions were performed under the optimal conditions of enzymes for 24 h, using glucuronoxylan and arabinoxylan as substrates. The generated soluble products were analyzed by HPAEC-PAD. (A) and (D): Standards: Solution containing xylooligosaccharides (XOS) from xylose ( $X_1$ ) to xylohexaose ( $X_6$ ). (B) Reaction products of rGH11XynB action on glucuronoxylan. (C) Reaction products of MetXyn11 action on glucuronoxylan. (E) Reaction products of rGH11XynB action on arabinoxylan. (F) Reaction products of MetXyn11 action on arabinoxylan. The results showed a clear difference between the cleavage patterns of MetXyn11 and rGH11XynB. MetXyn11 releases xylobiose as the only product from both substrates, whereas rGH11XynB generates several other xylooligosaccharides in addition to xylobiose. The results also showed the preference of MetXyn11 for less decorated heteroxylans, since the enzyme liberated much more xylobiose from glucuronoxylan (13% decorated) than arabinoxylan (40% decorated).

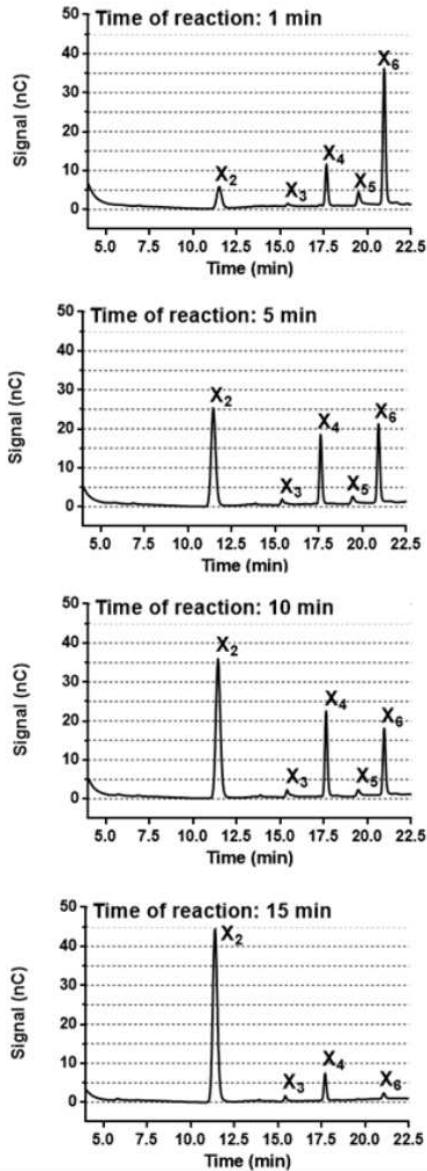


**Fig. 4: Cleavage pattern of MetXyn11 on xylooligosaccharides.** The MetXyn11 mechanism of action on homoxylan was assessed by HPAEC-PAD analysis, using xylohexaose as a model substrate. Reactions were conducted under the enzyme optimal conditions for 1, 5, 10 and 15 min. A profile of released xylooligosaccharides observed over a period of 15 min shows conversion of xylohexaose in xylotetraose plus xylobiose, and xylotetraose in two xylobioses, besides the conversion of xylopentaose in xylotriase plus xylobiose. Therefore, MetXyn11 cleaves and liberates xylobiose as the only product which is consistent with an exo-catalytic mechanism of the enzyme.

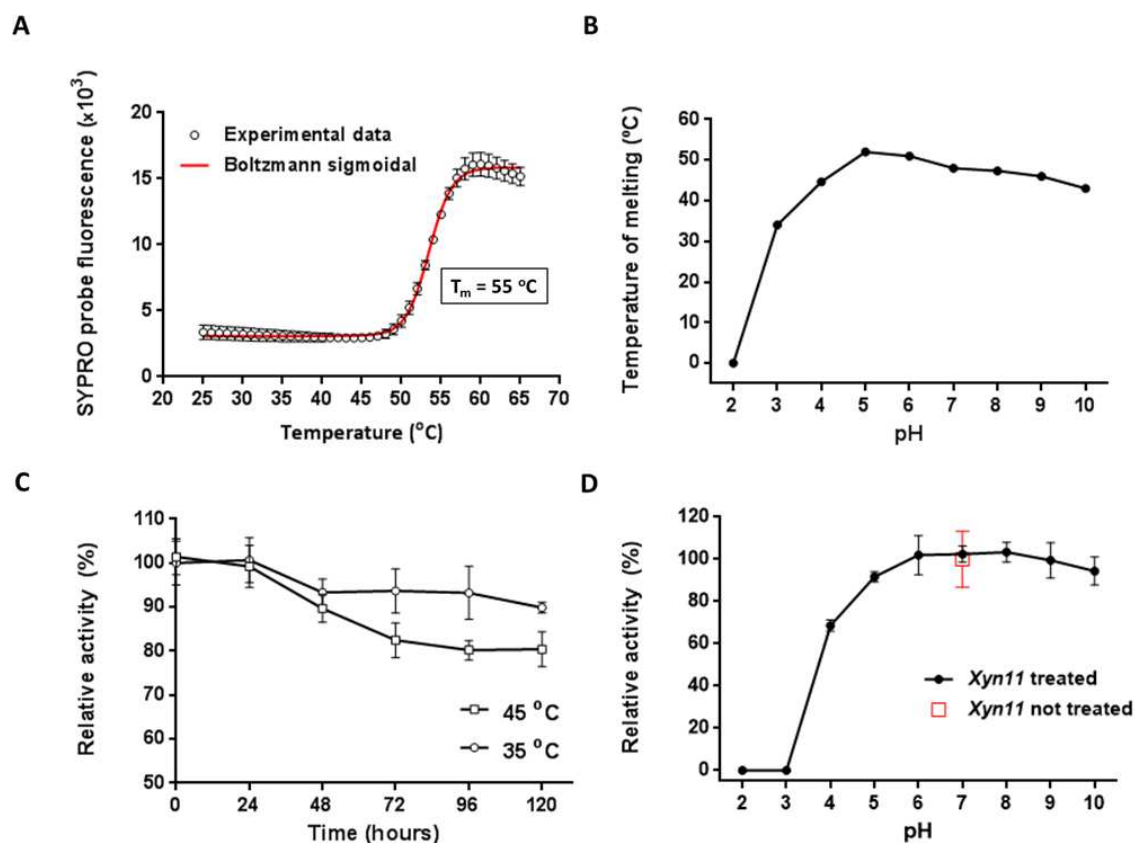


**Fig. 5: Thermal and pH stability of MetXyn11.** The thermal stability of MetXyn11 was assessed by both Thermofluor (A-B) and residual activity assays (C-D). In Thermofluor assay, MetXyn11 was exposed to a wide pH range during a linear increase in temperature until protein thermal denaturation. (A) At the optimal buffer condition (potassium phosphate pH 7.0) MetXyn11 has a  $T_m$  of 55  $^\circ\text{C}$ . (B) MetXyn11 has excellent pH stability in a wide range from pH 4 to 10 in ABF buffer. For residual activity assay, MetXyn11 activity was measured after keeping the enzyme for 120 h under the optimal conditions for its activity and also measured after 72 h at optimal temperature (50  $^\circ\text{C}$ ), but varying pH from 2 to 10. (C) The enzyme has good thermostability, maintaining 45% of its original activity after 96 h of incubation. (D) MetXyn11 also has good pH stability at pH 5-6 (above 70%).

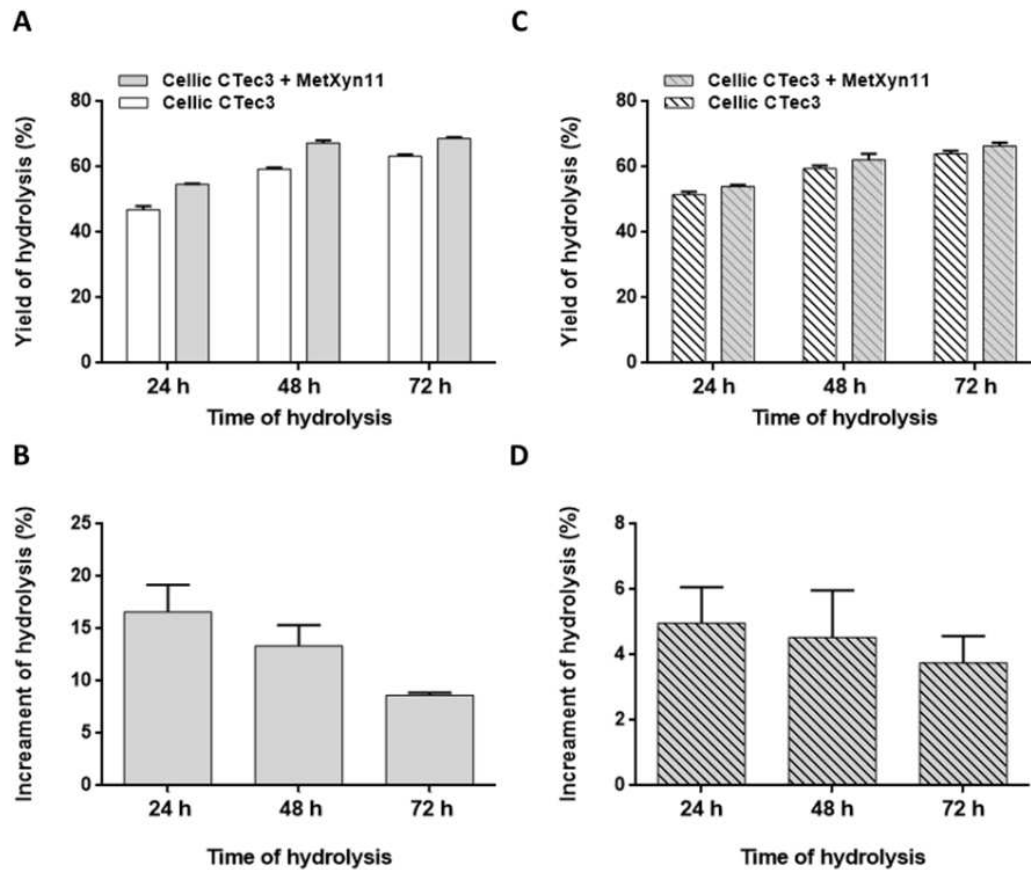


**Fig. 7: Yields of enzymatic hydrolysis of pretreated sugarcane bagasse.** Enhancement of commercial enzymatic cocktail Cellic CTec3 by addition of MetXyn11 was assessed by HPLC analyses of glucose and xylose under optimal CTec3 conditions of pH and temperature, using hydrothermal pretreated sugarcane bagasse as a substrate. (A) Yield of glucose release as a function of the time using Cellic CTec3 alone, and using a mixture of Cellic CTec3 plus MetXyn11. (B) The relative increments in the yields of released glucose as a function of the time. (C) Yield of xylose release as a function of the time using Cellic CTec3 alone and using a mixture of Cellic CTec3 plus MetXyn11. (D) The relative increments in the yields of released xylose as a function of the time.

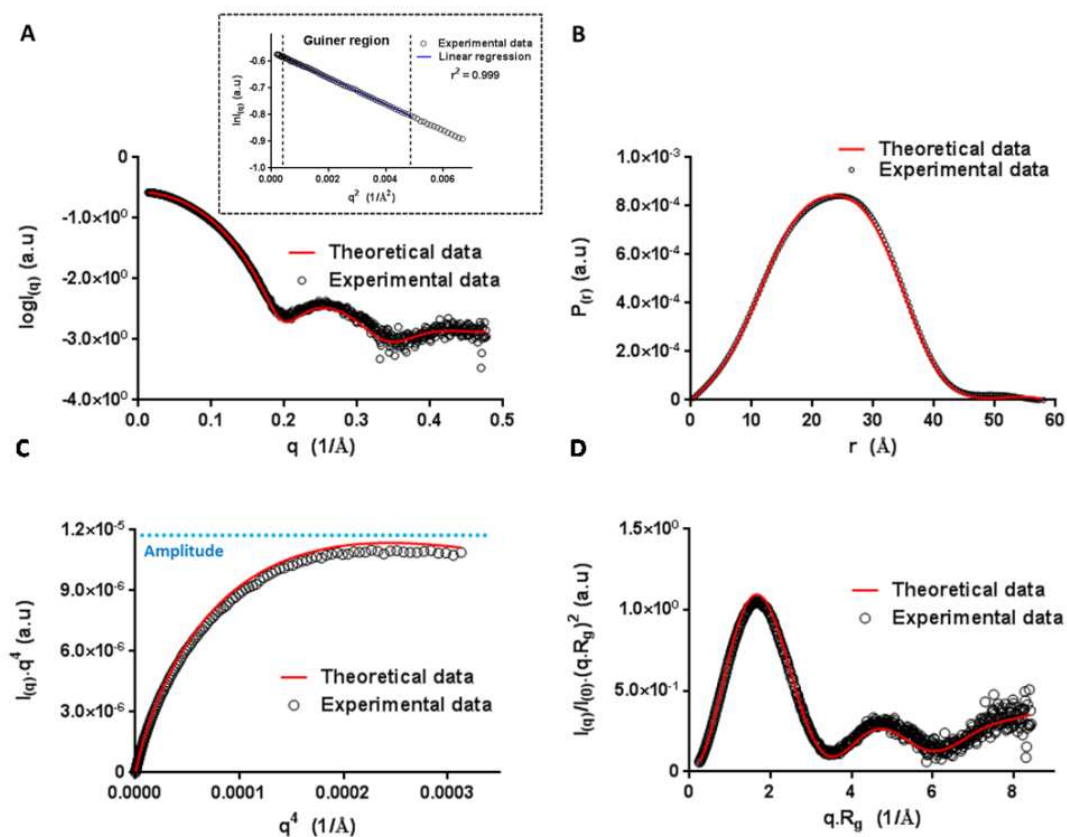


**Fig. 8: SAXS analysis.** (A) Experimental solution scattering profile superimposed with the theoretical scattering profile calculated based on MetXyn11 3D homology model. The insert figure shows that the Guinier plot data and the linear regression satisfy the approximation  $q < 1.3/R_g$ . (B) The  $p(r)$  plot displays an almost perfect bell-shape, including an extended tail with a small second peak at the highest  $q$ -region, indicating a small deviation of ellipsoidal shape. (C) Porod-Debye plot displays a clear plateau, expected for globular-like proteins that lack disordered regions. (D) The dimensionless Kratky plot presents a well-defined maximum that is consistent with a globular protein, and also presents a subtle elevated baseline at  $qR_g > 6$ , suggesting some flexibility of the protein structure.

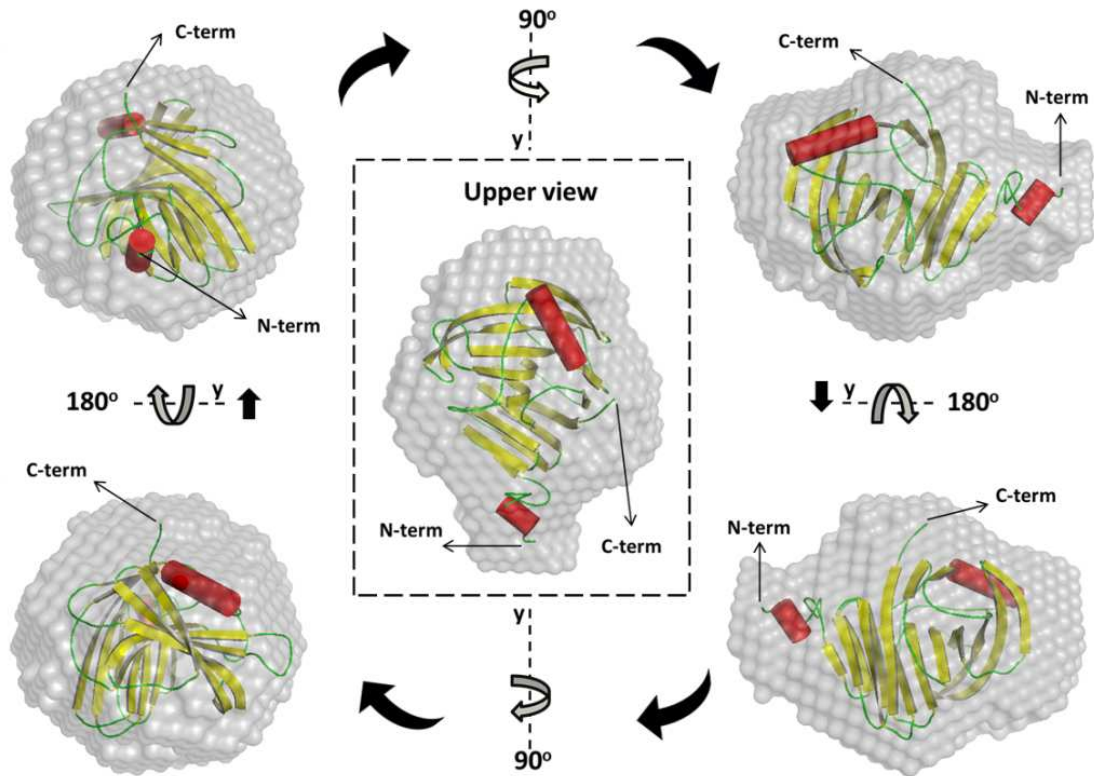


**Fig. 9: MetXyn11 low-resolution molecular envelope computed from experimental SAXS data.** The 3D-homology model of MetXyn11 (colored) was superposed into the average ab initio SAXS envelope (gray). The N-terminus (N-term) and C-terminus (C-term) of MetXyn11 are indicated for better orientation. The low-resolution envelope fits well the 3D homology model of MetXyn11, revealing a monomeric globular-like protein with a protuberance at its N-terminus.

**Applied Microbiology and Biotechnology**

**Supplementary Materials**

**Biochemical characterization and low-resolution SAXS shape of a novel GH11 exo-1,4- $\beta$ -xylanase identified in a microbial consortium**

**Danilo Elton Evangelista<sup>1a</sup>, Vanessa de Oliveira Arnoldi Pellegrini<sup>1a</sup>, Melissa Espirito Santo<sup>1</sup>, Simon McQueen-Mason<sup>2</sup>, Neil C. Bruce<sup>2</sup> and Igor Polikarpov<sup>1\*</sup>.**

<sup>1</sup>Instituto de Física de São Carlos, Universidade de São Paulo, Avenida Trabalhador São-carlense 400, 13566-590 São Carlos – SP, Brazil.

<sup>2</sup>Department of Biology, University of York, Wentworth Way, York, UK, YO10 5DD

<sup>a</sup>These authors contributed equally to this work

\*Corresponding author: [ipolikarpov@ifsc.usp.br](mailto:ipolikarpov@ifsc.usp.br), tel.: +55(16)3373-8088; fax: +55(16) 3373-9881

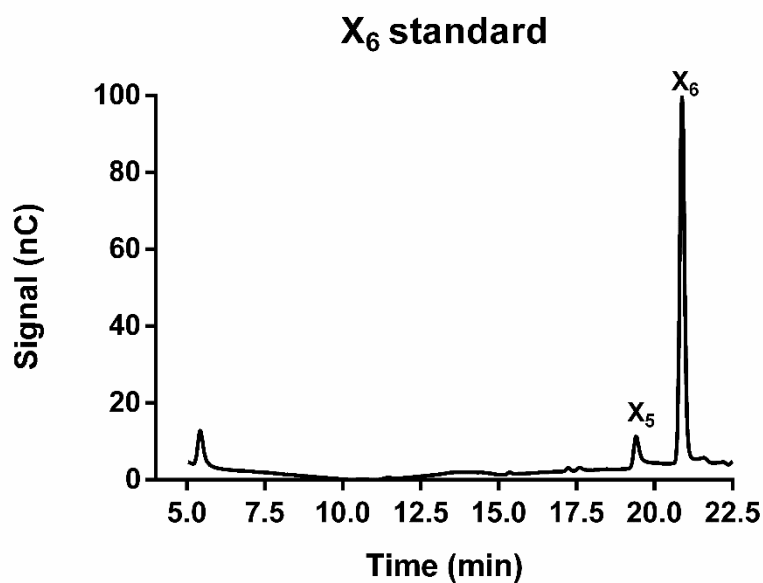


**Figure S1.** HPAEC-PAD analysis of xylohexaose (X<sub>6</sub>) standard. Small contamination with xylopentaose (X<sub>5</sub>) can be clearly visualized.

**Table S1. Thermofluor analysis.** Effect of different buffer solutions on tertiary structure stability of MetXyn11. Asterisk indicates the highest T<sub>m</sub> values.

pH	Buffer (50 mM)	T <sub>m</sub> (°C)
7.0	Control (water)	55*
1.2	HCl	26
2.0	HCl	45
3.0	Citric acid	26
4.0	Sodium citrate	46
4.5	Sodium acetate	48
4.7	Sodium citrate	51
5.0	Sodium acetate	52
5.0	Potassium phosphate	54
5.5	Sodium citrate	54
5.5	Sodium phosphate	55*
5.8	MES	55
6.0	Potassium phosphate	54
6.0	Bis-Tris	55*
6.2	MES	55*
6.5	Sodium phosphate	53
6.5	Sodium cacodylate	54
6.5	Bis-Tris	55*
6.5	MES	55*

6.7	Bis-Tris	55*
7.0	Potassium phosphate	53
7.0	HEPES	55*
7.0	Bis-Tris	55*
7.3	Amonium acetate	54
7.5	Sodium phosphate	50
7.5	Tris	54
8.0	Imidazole	52
8.0	HEPES	52
8.0	Tris	52
8.0	Bicine	52
8.5	Tris	51
9.0	Bicine	49
9.5	Sodium carbonate	46
10.0	Sodium carbonate	45

---

**Table S2. Metal ions and chemicals influence.** The effects of the metal ions, reducing agents and surfactants on MetXyn11 enzymatic performance were assessed and compared with other GH11 xylanases. N/A = Not available.

Enzyme name	MetXyn11	Xyn11A	Xyn11B	Xyn11B119
Organism	Unknown	<i>P. oxalicum</i>	<i>P. oxalicum</i>	<i>Streptomyces sp.</i>
Reference	Present study	Liao et al. 2015	Liao et al. 2015	Zhou et al., 2011
<b>Metal ions</b>	<b>Residual activity (%)</b>			
	(10 mM)	(10 mM)	(10 mM)	(10 mM)
Control	100.0 ± 1.8	100.0 ± 3.7	100.0 ± 0.6	100.0 ± 2.6
Ca <sup>+2</sup>	81.3 ± 4.2	118.9 ± 1.7	100.1 ± 3.4	98.3 ± 5.1
Co <sup>+2</sup>	79.0 ± 6.8	124.9 ± 2.5	81.7 ± 1.6	97.3 ± 2.8
Cu <sup>+2</sup>	54.3 ± 1.7	2.3 ± 0.16	41.6 ± 2.6	N/A
Fe <sup>+2</sup>	53.6 ± 3.5	115.5 ± 3.1	101.3 ± 2.5	101.0 ± 1.6
Fe <sup>+3</sup>	0.50 ± 0.7	22.8 ± 1.0	33.0 ± 0.5	N/A
Mn <sup>+2</sup>	21.9 ± 10.3	108.8 ± 2.8	100.1 ± 2.7	65.6 ± 0.9
Mg <sup>+2</sup>	123.1 ± 6.9	127.6 ± 2.0	101.8 ± 2.7	99.0 ± 0.8
Ni <sup>+2</sup>	110.2 ± 1.6	116.1 ± 2.5	79.1 ± 3.1	122.3 ± 2.8
K <sup>+</sup>	112.3 ± 10.3	N/A	N/A	101.4 ± 2.6
Li <sup>+2</sup>	106.1 ± 6.35	119.4 ± 2.3	89.6 ± 3.9	101.3 ± 3.6
<b>Reducing agents</b>	<b>Residual activity (%)</b>			
	(1 mM)	(1 mM)	(1 mM)	(10 mM)
β-Mercaptoethanol	84.8 ± 0.9	41.7 ± 0.1	101.0 ± 5.3	126.5 ± 2.0
DTT	95.1 ± 1.7	100.2 ± 1.2	98.3 ± 2.6	N/A
<b>Surfactants</b>	<b>Residual activity (%)</b>			
	(0.1%)	(0.1%)	(0.1%)	(0.3%)
Tween-20	83.5 ± 0.3	100.8 ± 1.2	104.6 ± 7.6	N/A
Triton-100X	107.9 ± 0.4	100.0 ± 1.1	88.8 ± 2.9	N/A
SDS	0.0 ± 0.0	23.9 ± 1.8	3.5 ± 0.3	110.8 ± 7.2

**Table S3. SAXS data collection and processing.**

<b>Data collection</b>	
Beamline	LNLS-SAXS1
Wavelength (Å)	1.55
q range (Å <sup>-1</sup> )	0.0138 – 0.47699
Exposure time per frame (s)	30
Concentration range (mg.mL <sup>-1</sup> )	1.0, 3.5 and 15.0
Temperature (°C)	20
<b>Data Analysis</b>	
I <sub>(0)</sub>	0.26 ± 0.00
Guinier q-region (Å <sup>-1</sup> )	0.0138 – 0.06983
R <sub>g</sub> (Å) from Guinier (± SE)	18.52 ± 0.04
R <sub>g</sub> (Å) from GNOM (± SE)	17.67 ± 0.06
D <sub>max</sub> (Å)	58
Resolution (2π.q <sub>max</sub> <sup>-1</sup> ) (Å)	13.17
Oligomeric state	Monomer
<b>Ab initio modeling</b>	
Number of models	10
NSD	0.572 ± 0.008
<b>Software employed</b>	
Primary data reduction	Fit2D
Data processing	Primus
Theoretical data fitting	Crysol
Envelope modeling	Dammin
3D-Homology modeling	I-Tasser

